Kinase Chemodiversity from the Arctic: The Breitfussins

Kine Ø. Hansen,[1,*] Jeanette H. Andersen,[1] Annette Bayer,[2] Sunil K. Pandey,[3,†] Marianne Lorentzen,[4] Kåre B. Jørgensen,[4] Magne O. Sydnes,[4] Yngve Guttormsen,[2] Matthias Baumann,[5] Uwe Koch,[5] Bert Klebl,[5] Jan Eickhoff,[5] Bengt Erik Haug,[3,*] Johan Isaksson,[2] and Espen H. Hansen[1]

[1]Marbio, UiT - The Arctic University of Norway, Breivika, NO-9037 Tromsø, Norway

[2]Department of Chemistry, UiT - The Arctic University of Norway, Breivika, NO-9037 Tromsø, Norway

[3]Department of Chemistry and Centre for Pharmacy, University of Bergen, Allégaten 41, NO-5007 Bergen, Norway

[4]Faculty of Science and Technology, Department of Chemistry, Bioscience and Environmental Engineering, University of Stavanger, NO-4036, Stavanger, Norway

[5]Lead Discovery Center GmbH, Otto-Hahn-Strasse 15, 44227, Dortmund, Germany

ABSTRACT. In this work, we demonstrate that the indole-oxazole-pyrrole framework of the breitfussin family of natural products is a promising scaffold for kinase inhibition. Six new halogenated natural products, breitfussin C – H (**3** – **8**) were isolated and characterized from the Arctic, marine hydrozoan *Thuiaria breitfussi*. The structures of two of the new natural products were also confirmed by total synthesis. Two of the breitfussins (**3** and **4**) were found to selectively inhibit the survival of several cancer cell lines, with the lowest IC_{50} value of 340 nM measured against the drug-resistant triple negative breast cancer cell line MDA-MB-468, while leaving the majority of the tested cell lines not or significantly less affected. When tested against panels of protein kinases, **3** gave IC_{50} and K_d values as low as 200 and 390 nM against the PIM1 and DRAK1 kinases, respectively. The activity was confirmed to be mediated through ATP competitive binding in the ATP binding pocket of the kinases. Furthermore, evaluation of potential off-target and toxicological effects, as well as relevant *in vitro* ADME parameters for **3** revealed that the breitfussin scaffold holds promise for the development of selective kinase inhibitors.

INTRODUCTION

The human genome encodes 538 protein kinases, many of which are known to have fundamental roles in the molecular machinery controlling cell proliferation, survival and motility.[1] As these processes are tightly regulated in normal cells, mutations causing dysregulation of kinase functions have been linked to a wide range of human malignancies.[1-3] Several small-molecule kinase inhibitors have been marketed as drugs to treat a variety of different cancers, including leukemia and gastrointestinal tumors.[4, 5] Inhibition of kinase activity using selective inhibitors provides a targeted treatment option with overall fewer side effects compared to traditional cancer chemotherapeutics.[6] As most kinase inhibitors bind to the highly conserved ATP-binding pocket, development of selective inhibitors is challenging.[7, 8] Accordingly, new scaffolds for selective kinase inhibition are in high demand.

The breitfussins are a family of highly modified halogenated compounds comprising a unique indole-oxazole-pyrrole molecular framework. The first two compounds, breitfussin A and B (**1** and **2**, Figure 1), were isolated from the cnidarian *Thuiaria breitfussi* and reported by us in 2012.[9]
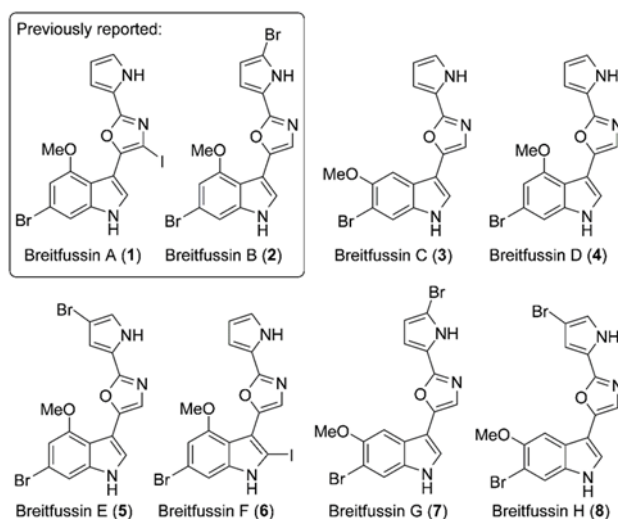

Figure 1. Structures of **1** – **8**.

Due to the low number of protons compared to heavy atoms (ratio 1:2), the structures of **1** and **2** could not be elucidated by traditional methods alone, and atomic force microscopy (AFM) was used for the first time to elucidate the structure of unknown natural products.[9] The structures of **1** and **2** were later confirmed by total synthesis.[10] Natural products consisting of oxazole-pyrrole[11] or indole-oxazole[12-14] moieties have previously been reported, however, the breitfussins are the first examples of natural products containing all three heterocycles.

In the present work, we describe further chemical investigation of the organic extracts of *T. breitfussi* which led to the characterization of six new breitfussin analogues, breitfussin C – H (**3** – **8**, Figure 1). Previously, bioactivity data (against one colon cancer cell line, bacteria- and fungal strains) for synthetically produced **2** has been reported by others,[15, 16] while no bioactivity data has been reported for **1** and **3** – **8**. We herein report on the cytotoxic activity against cancer cell lines and kinase inhibition profiles of **1** – **6**. Further, we report the total synthesis of **3** and **4**, which followed a similar strategy as reported for **1** and **2**.[10] Based on initial bioactivity data we performed an extended evaluation of the pharmacological potential of **3**, and the potential of the core structure of the breitfussins as a new ATP-competitive kinase inhibitor scaffold was demonstrated.

RESULTS AND DISCUSSION

Isolation and Structural Elucidation

Specimens of *T. breitfussi* (475.6 g) were collected near Bjørnøya (Barents Sea) during a research cruise in 2011. We have previously reported the isolation and structure elucidation of **1** and **2** from a different *T. breitfussi* sample collected in the same area in 2007.[9] Repeated purification of the organic *T. breitfussi* extract, using semi-preparative HPLC, led to the isolation of eight related compounds. Two of these were confirmed to be **1** and **2**, while **3** - **8** were determined to be new breitfussin analogues.

Breitfussin C (**3**) was isolated as a light brown powder. HRMS analysis suggested a molecular formula of $C_{16}H_{12}BrN_3O_2$ (12 degrees of unsaturation, *m/z* 358.0195 $[M+H]^+$, Δmmu = 0.4). The ^{1}H NMR spectrum of **3** (Table 1) recorded in DMSO-d_6 displayed signals for seven aromatic protons with chemical shift values ranging from 7.79 to 6.18, two exchangeable protons at δ_H = 11.85 and 11.64, as well as signals for one methyl group attached to a heteroatom at δ_H 3.91. The ^{13}C NMR spectrum of **3** (Table 2) confirmed the presence of 16 carbon atoms, including one methyl, seven methine and eight quaternary carbon atoms. The NMR spectra of **3** revealed chemical shifts in close agreement with those of **1** and **2**. HMBC and HSQC experiments were used to determine the substitution pattern of the breitfussin skeleton of **3** (Figure 2). In the HMBC spectrum of **3**, the methoxy protons (δ_H = 3.91) correlated with C-6 (δ_C 150.31). The downfield shift of C-6 in **3** is in agreement with the shift expected for a methoxylation in this position, and was also confirmed by a NOE between H-5 (δ_H = 7.38) and the methoxy protons (δ_H = 3.91). C-7 (δ_C 107.1) was quaternary and attachment of the bromine atom to C-7 completed the planar structure of **3**. The structure of **3** was hence assigned as 5-(6-bromo-5-methoxy-1*H*-indol-3-yl)-2-(1*H*-pyrrol-2-yl)oxazole.
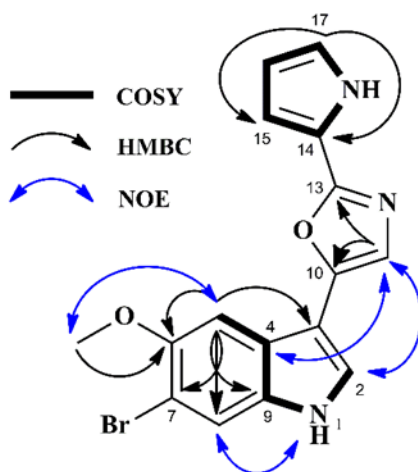

Figure 2. Selected COSY, HMBC and NOE correlations obtained for **3**.

Breitfussin D (**4**) was isolated as a pale brown oil. Its molecular formula was found to be $C_{16}H_{12}BrN_3O_2$ (12 degrees of unsaturation, *m/z* 358.0197 [M+H]$^+$, Δmmu = 0.6) on the basis of HRMS analysis. The ^{1}H NMR spectrum of **4** recorded in DMSO-d_6 (Table 1) displayed two NH signals: H-18 at δ_H = 11.79 and H-1 at δ_H = 11.75, along with a signal for one methoxy group at δ_H 3.95 and for seven aromatic protons with shift values ranging from δ_H 7.44 – 6.20. The ^{13}C NMR spectrum of **4** confirmed the presence of 16 carbon atoms including one methyl, seven methines and eight quaternary carbon atoms, further supporting the breitfussin carbon framework (Table 2).

Table 1. Summary of ^{1}H NMR (600 MHz, (CD$_3$)$_2$SO) data for **3 – 8**.

position	**3** δ_H (*J* in Hz)	**4** δ_H (*J* in Hz)	**5** δ_H (*J* in Hz)	**6** δ_H (*J* in Hz)[#]	**7** δ_H (*J* in Hz)[#]	**8** δ_H (*J* in Hz)[#]
1	11.64, d (2.6)	11.75, s	12.00, s	12.25, s	11.55, s	11.55, s
2	7.79, d (2.7)	7.74, s	7.76, s		7.83, s	7.83, s
5	7.38, s				7.42, s	7.42, s
6		6.73, d (1.6)	6.73,d (1.6)	6.67, d (1.4)		
8	7.67, s	7.25, d (1.6)	7.26,d (1.6)	7.13, d (1.4)	7.70, s	7.77, s
11	7.50, s	7.34, s	7.36, s	7.18, s	7.56, s	7.58, s
15	6.72, ddd (3.8, 2.4, 1.6)	6.72,ddd (3.7, 2.0, 1.4)	6.78,d (1.4)	6.66, dd (3.7, 1.5)	6.74, d (3.8)	6.80, d (1.7)
16	6.18, dt (3.5, 2.4)	6.20, dt (3.5, 2.3)		6.16, dd (3.7, 2.6)	6.27, d (3.8)	
17	6.94, td (2.6, 1.5)	6.97, td (2.6, 1.5)	7.11, d (1.4)	6.91, dd (2.6, 1.5)		7.13, d (1.7)
18	11.85, s	11.79, s	12.30, s	11.77, s	12.61, s	12.20, s
-OMe	3.91, s	3.95, s	3.95, s	3.75, s	3.95, s	3.95, s

[#]Couplings measured in MeOD for better resolution

Table 2. Summary of ^{13}C NMR (151 MHz, $(CD_3)_2SO$) data for **3 – 8**.

	3	**4**	**5**	**6**	**7**	**8**
position	δ_C, type	δ_C, type	δ_C, type	δ_C, type	δ_C, type	δ_C, type
2	124.7, CH	123.6, CH	124.0, CH	84.4[#], C	125.0, CH	125.0, CH
3	104.3, C	104.5, C	104.2, C	109.1[#], C	104.1, C	104.1, C
4	123.6, C	113.1, C	113.2, C	116.2[#], C	123.5, C	123.5, C
5	102.2, CH	154.0, C	154.1, C	152.6, C	102.2, CH	102.2, CH
6	150.3, C	104.3, CH	104.4, CH	107.0, CH	150.4, C	150.4, C
7	107.1, C	115.7, C	115.8, C	115.8, C	107.1, C	107.1, C
8	116.6, CH	108.4, CH	108.5, CH	104.1, CH	116.6, CH	116.6, CH
9	132.0, C	138.9, C	139.0, C	141.2[#], C	132.0, C	132.0, C
10	145.9, C	146.1, C	nd	144.6, C	146.2, C	146.2, C
11	120.5, CH	123.8, CH	123.1, CH	126.2, CH	120.5, CH	120.5, CH
13	154.4, C	154.6, C	153.3, C	155.8, C	153.2, C	153.2, C
14	120.3, C	120.5, C	121.4, C	120.3, C	122.2, C	121.3, C
15	109.8, CH	109.6, CH	111.0, CH	109.6, CH	111.2, CH	111.1, CH
16	109.7, CH	109.7, CH	96.3, C	109.5, CH	111.9, CH	96.4, C
17	122.0, CH	121.8, CH	121.6, CH	122.0, CH	102.4, C	121.6, C
-OMe	57.0, CH_3	56.1, CH_3	55.9, CH_3	55.7, CH_3	57.1, CH_3	57.1, CH_3

[#]Acquired at pH 3.5

Comparison of the ^{1}H and ^{13}C NMR spectra as well as HMBC coupling patterns of **4** with those of **1 – 3** confirmed the breitfussin skeleton. The downfield shift value of C-5 (δ_C 154.0) in **4** indicated methoxylation in this position of **4**. Correlations between the methoxy protons ($\delta_H = 3.95$) and C-5 (δ_C 154.0) in the HMBC spectrum of **4** confirmed the position of the methoxy group. As

for **3**, C-7 (δ_C 115.7) was substituted with the bromine atom, thus giving the full structure of **4** as 5-(6-bromo-4-methoxy-1*H*-indol-3-yl)-2-(1*H*-pyrrol-2-yl)oxazole.

Breitfussin F (**6**) was isolated as a light brown powder. HRMS analysis gave a molecular formula of $C_{16}H_{11}BrIN_3O_2$ (12 degrees of unsaturation, *m/z* 483.9161 [M+H]$^+$, Δmmu = 0.4). The ^{1}H NMR spectrum of **6** (Table 1) revealed the presence of a methoxy group (δ_H 3.75), four aromatic singlets (δ_H 7.18 – 6.16) and one NH proton H-18 (δ_H = 11.77). The NH-1 (δ_H 12.25) hydrogen could initially not be detected through NMR analysis. Due to the low amount of isolated material, only 12 out of 16 carbon atoms in **6** gave detectable signals through ^{13}C NMR analysis. The chemical shift of C-4 (δ_C = 116.0) was obtained through HMBC analysis, where it was found to correlate to H-6 (δ_H = 6.67) and H-8 (δ_H = 7.13). For C-2, C-3 and C-9, no cross peaks could be observed in the HMBC spectrum (Table 2). Through the 2D NMR experiments, partial structures of **6** could be unambiguously assembled: The pyrrole and the oxazole ring constituted one fragment and carbon atoms 4 to 8, including the methoxy group on the 5 position of the indole another fragment. This strongly indicates that **6** contains the characteristic breitfussin framework and leaves only one possibility for positioning of the iodine, i.e. on C-2 of the indole ring. An iodine at the C-2 position could explain the disappearance of the NH-1 proton as the iodine is expected to make the neighboring NH more acidic. Indeed, lowering the pH of the NMR sample to 3.5 shifted the equilibrium to protonating the nitrogen completely and the NH-1 did emerge at δ_H = 12.41 ppm. In this sample, the missing carbon shifts could be found at δ_C (C-2) = 84.4, δ_C (C-3) = 109.1, δ_C (C-4) = 116.2 and δ_C (C-9) = 141.2. The structure of **6** was therefore assigned as 5-(6-bromo-2-iodo-4-methoxy-1*H*-indo-3-yl)-2-(1*H*-pyrrol-2-yl)oxazole.

Breitfussin G (**7**) and H (**8**) could not be chromatographically separated using semi-preparative HPLC and were isolated together as a pale yellow liquid. UHPLC-HRMS analysis of **7** and **8** gave a molecular formula of $C_{16}H_{11}Br_2N_3O_2$ (12 degrees of unsaturation, **7**: *m/z* 435.9302 [M+H]$^+$,

Δmmu = 0.6; **8**: *m/z* 435.9303 [M+H]$^+$, Δmmu = 0.7) for both compounds. Comprehensive analysis of 1D (Table 1 and 2) and 2D NMR data, similar to the analysis performed for **6**, confirmed the breitfussin skeleton of **7** and **8** to be related to **3**. The methoxy group was in the 6 position, as in **3**, but an extra bromine was positioned on the pyrrole. In **7**, the bromine was placed on the C-17 based on H-15 and H-16 being vicinal as proved by a 3.8 Hz coupling and a strong ROE$_{H-15/H-16}$. In **8**, the bromine was placed on the C-16, resulting in the absence of any ROE$_{H-15/H-16}$ and a weaker $^4J_{H-15/H-17}$ of 1.7 Hz. The structure of **7** was therefore assigned as 2-(4-bromo-1*H*-pyrro-2-yl)-5-(6-bromo-5-methoxyl-1*H*-indol-3-yl)oxazole and **8** was assigned as 2-(5-bromo-1*H*-pyrrol-2-yl)-5-(6-bromo-5-methoxyl-1*H*-indol-3-yl)oxazole.

The structures of re-isolated **1** and **2** were confirmed by comparing the analytical data with those previously reported by us (Table S1 and S2).[9]

Total Synthesis of **3** and **4**

In order to carry out an extensive evaluation of the biological activity of **3**, additional material was required. Previously we have reported the synthesis of **1** and **2**[10] and the same strategy was applied for the synthesis of **3**. This time, the total synthesis commenced by TIPS-protection of 5-methoxyindole (**9**) following a literature procedure forming indole **10** (see SI).[17-19] Selective bromination of **10** (Scheme 1) by directed *ortho* metalation[20] proved to be difficult and several approaches including temporary introduction of a TMS group on C-3[21, 22] to induce steric hindrance,[22] use of TBS instead of TIPS as protection group and the use of different lithiation reagents failed to give 6-bromoindole **11** selectively.

**Scheme 1.** Total synthesis of **3** from indole **10**[a]
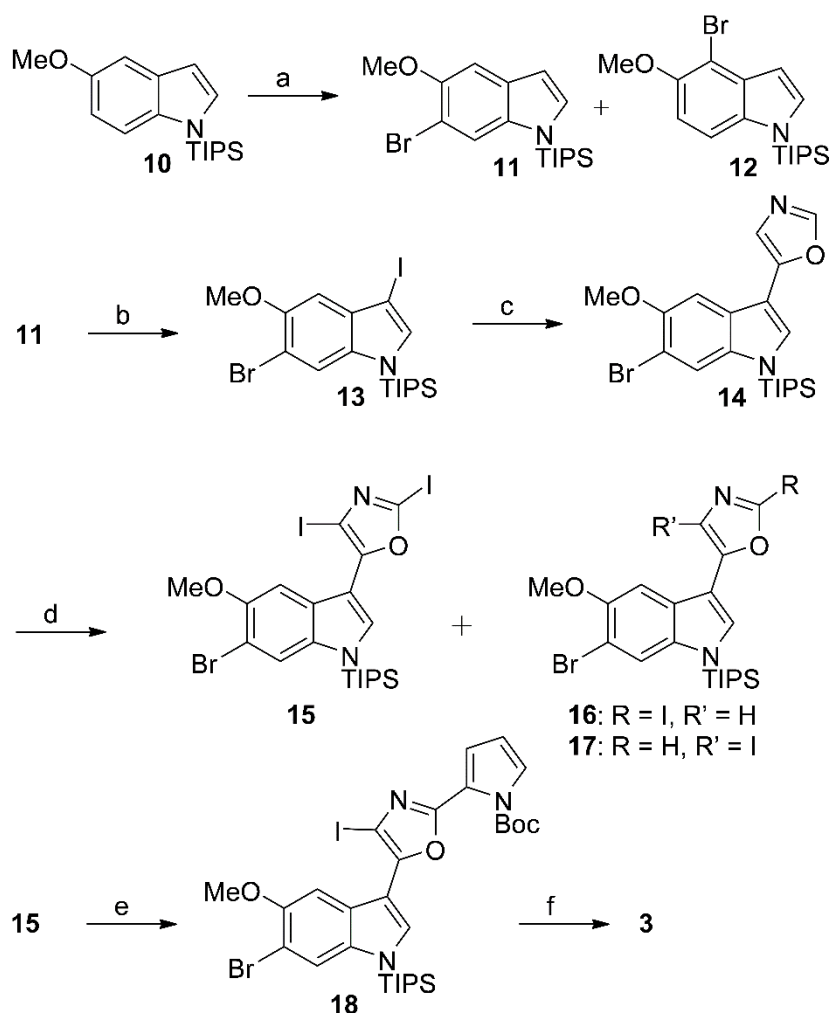
[a]Reagents and conditions: (a) i) *sec*-BuLi, TMEDA, THF, 15 °C to -5 °C ii) Br(CH₂)₂Br, -5 °C to rt (67%yield for mixture of **11** and **12**); (b) ICl, pyridine, CH₂Cl₂, 0 °C to rt (97% yield); (c) i) (2-triisopropylsilyl)oxazol-5-yl)boronic acid pinacol ester, Pd(dppf)Cl₂, K₃PO₄, toluene/H₂O, 80 °C, ii) 10% aq. HCl, THF, 0 °C (62% yield over 2 steps); (d) i) LiHMDS, THF, -78 °C ii) I₂, -78 °C (31% yield for **15**, 47% yield for mixture of **16** and **17**); (e) *N*-Boc-pyrrole-2-boronic acid, Pd(dppf)Cl₂•CH₂Cl₂, Cs₂CO₃, dioxane/H₂O (66% yield); (f) i) TFA, CH₂Cl₂, 0 °C to rt, ii) TBAF, THF (68% yield over 2 steps).

Eventually we found that using *sec*-BuLi/TMEDA followed by a reaction with 1,2-bromoethane gave a 2:3 mixture of 6-bromoindole **11** and 4-bromoindole **12** in 67% combined yield. **11** could then be isolated in pure form in 14% yield by crystallization from hexane. 6-Bromoindole **11** could

then be iodinated to give **13** in high yield, which was subsequently submitted to the optimal coupling conditions identified in our previous synthesis of **1** and **2**. Treating the cross-coupling product directly with aqueous HCl resulted in selective deprotection of the TIPS group in 2-position on the oxazole giving oxazole **14** in good yield. In our earlier synthesis of **1** and **2**, we could only successfully couple onto a 2,4-diiodo oxazole derivative and not the 2-iodo oxazole derivative, thus 2,4-diiodo oxazole **15** was the target for the next step. The iodination of **14** however proved to be sluggish, and similarly as reported earlier for the iodination *en route* to **1** and **2**,[10] we ended up with a mixture of the desired diiodo product **15** in 31% yield in addition to substantial amounts of mono-iodinated oxazoles **16** and **17** (47% combined yield of **16** and **17**). Mono-iodinated oxazoles **16** and **17** were not separable by flash chromatography and re-submitting a mixture of **16** and **17** to the reaction conditions gave **15** in 61% yield. This provided sufficient amounts of the desired material and further Suzuki-Miyaura cross-coupling of **15** with Boc-protected 2-pyrrolyl boronic acid gave the complete indole-oxazole-pyrrole scaffold **18** in good yield. Finally, **18** was submitted to simultaneous acid-mediated Boc-deprotection and deiodination followed by TIPS deprotection to give **3** in 1.1% yield over 9 steps. Deiodination and deprotection of the earlier reported intermediate **19** (Scheme 2)[10] gave natural product **4**, which has been prepared previously by another group using a different approach.[16]

Scheme 2. Synthesis of **4**[a]
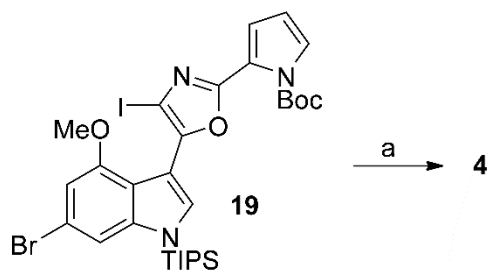
[a]Reagents and conditions: (a) i) TFA, CH₂Cl₂, 0 °C to rt, ii) TBAF, THF (77% yield over 2 steps).

In vitro Cytotoxic Activities of **1 – 6**

The cytotoxic properties of **1 – 6** were evaluated against seven cancer cell lines (MCF-7, MDA-MB-468 and SK-BR-3: breast adenocarcinoma, HT-29: colon adenocarcinoma, MOLT-4 and MV-4-11: leukemia and A2058: melanoma,) and one non-malignant cell line (MRC-5: lung fibroblasts) (Table 3) using the MTS assay.[23] Compounds **7** and **8** were not evaluated, as they were isolated as a mixture.

Table 3. IC$_{50}$ (μM) of **1 – 6** against seven malignant and one non-malignant cell line.

Comp	IC$_{50}$ (μM) $\pm$ SD							
	MCF-7[b]	MDA-MB-468[b]	SK-BR-3[b]	HT-29[c]	MOLT-4[d]	MV-4-11[e]	A2058[f]	MRC-5[g]
1	na[a]	na	na	na	na	na	na	na
2	na	na	na	na	na	na	na	na
3	8.5 $\pm$ 0.2	na	na	7.1 $\pm$ 0.2	9.9 $\pm$ 0.4	4.4 $\pm$ 0.5	na	7.1 $\pm$ 0.6
4	3.9 $\pm$ 0.3	na	na	na	na	na	na	na
5	na	na	na	na	na	na	na	na
6	na	na	na	na	na	na	na	na

[a]na: not active (IC$_{50}$ > 10 μM); [b]MCF-7, MDA-MB-468 and SK-BR-3: breast adenocarcinoma; [c]HT-29: colorectal adenocarcinoma; [d]MOLT-4: acute lymphoblastic leukemia, [e]MV-4-11: myelomonocytic leukemia; [f]A2058: melanoma; [g]MRC-5: non-malignant lung fibroblasts, all of human origin.

While **1**, **2**, **5** and **6** showed no significant activity towards these cell lines, **3** and **4**, displayed cytotoxic activities. Compound **3** reduced the viability of MCF-7, HT-29, MOLT-4, MV-4-11 and MRC-5, and **4** affected the viability of MCF-7. Only IC$_{50}$ values under 10 μM were measurable, as the compound precipitated at around 20 μM in this assay setup, interfering with the readout of the experiments. Through microscopic evaluation of test wells it was however clear that the sensitivity

of the cells towards the compounds varied significantly. For example, compound **3** had no observable effect towards A2058 viability at concentrations up to 100 μM.

To evaluate whether the activities of **3** and **4** were time-dependent, IC_{50} values for the compounds were determined after 4, 24, 48 and 72 h of exposure against two cell lines (**3** against HT-29, **4** against MCF-7). Exposure of the affected cell lines to **3** and **4** gave decreasing IC_{50} values with increasing exposure times (Figure S3).

The Breitfussins as Kinase Inhibitors

To identify potential cellular targets of the breitfussins, **1**, **3** and **4** were tested against a panel of 140 kinases at the International Centre for Kinase Profiling (ICKP) in Dundee (Scotland, UK) using activity-based radioactive (^{33}P-ATP) filter-binding assays.[24] Compound **1** was tested at 50 μM, **3** at 50, 5 and 1 μM and **4** at 5 and 1 μM (Table S3). At 50 μM, **1** was the least active of the tested compounds. Three kinases had residual enzyme activities (RA) between 50 and 30% and two below 30% (AMPK: 28%, TSSK1: 21%). Compound **1** was therefore not tested at lower concentrations. At 50 μM, **3** gave RAs between 50 and 30% for 23 kinases, between 30 and 10% for 24 kinases and lower than 10% for 7 kinases (RIPK2: 10%, ERK8: 9%, GCK: 7%, TAK1: 7%, Aurora B: 6%, MLK1: 5% and PIM1: 2%) (Figure 3A). At 5 μM, the number of kinases inhibited by **3** decreased and at 1 μM, **3** gave RAs between 50 and 30% for 5 kinases (NUAK1: 46%, RIPK2: 41%, TAK1: 35%, Aurora B: 33%, GCK: 31%), between 30 and 10% for 2 kinases (MLK1: 26%, MLK3: 20%) and lower than 10% for 2 kinases (PIM1: 6%, PIM3: 7%) (Figure 3B). At 5 μM, **4** affected 3 kinases to give RAs between 50 and 30%, 5 kinases between 30 and 10% and 2 kinases to RAs lower than 10% (MLK1: 7%, MLK3: 7%), while at 1 μM, no kinase had RAs below 10%, and one kinase had a RA below 30% (PIM3: 29%).
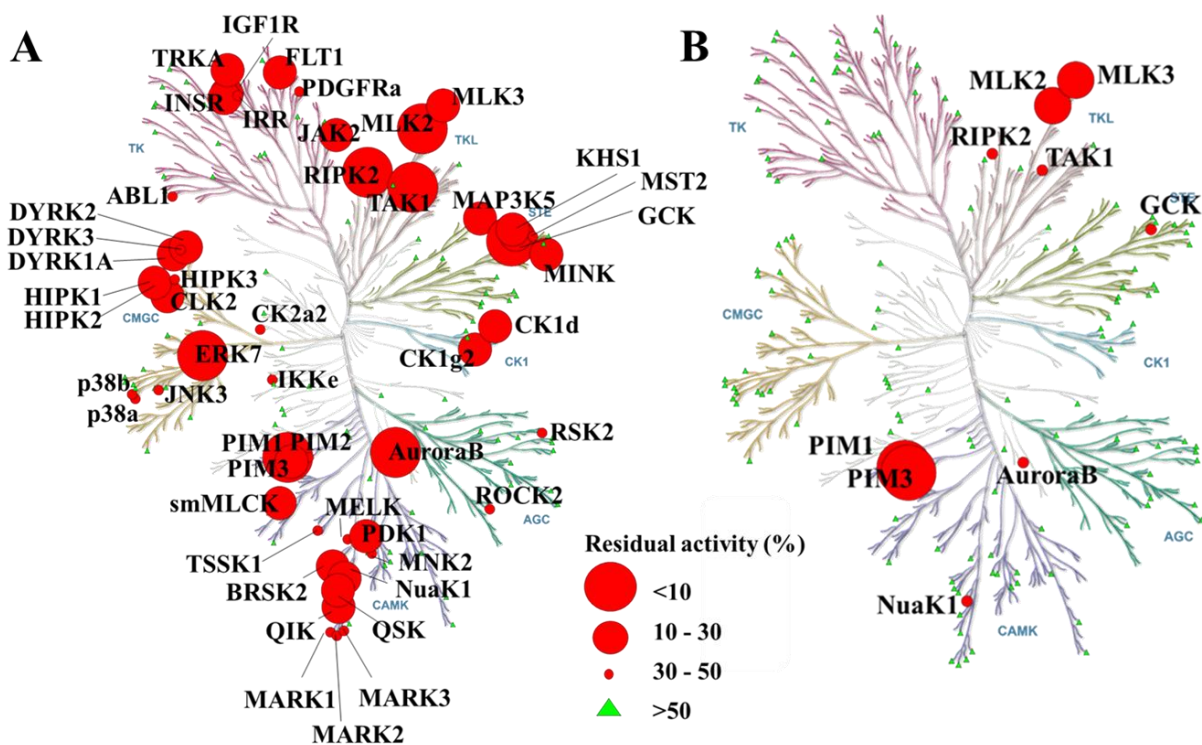
Figure 3. Kinome inhibition data of **3** at 50 (A) and 1 µM (B) against 140 kinases. Disc sizes and colors are encoding the level of residual activity as shown in figure key.

Selectivity of Breitfussin Kinase Inhibition

From the data obtained through the kinase inhibition experiments, it was possible to draw Lorenz curves and calculate the Gini coefficient (GC)[25] for **3** at 50, 5 and 1 µM and for **4** at 5 µM. The GC of **3** rose from 0.432 at 50 µM to 0.484 at 5 µM, and 0.605 at 1 µM. The GC for **4** at 5 µM was 0.529. The GC for **4** at 1 µM could not be calculated, as too few kinases were affected. The GC score of 0.605 for **3** at 1 µM is high for a natural product whose scaffold has not been optimized through synthesis. It is worth mentioning that lapatinib, gefitinib and sunitinib, which are all marketed kinase inhibitors used to treat various types of cancers, have GC scores of 0.57, 0.65 and 0.67, respectively, when assayed against 317 kinases at 10 µM.[26, 27] GC scores do not take into account selectivity for subsets of related kinases, and the scores cannot be directly compared to

other compounds unless tested under the same conditions (same concentration, same panel of kinases etc.). However, it provides an overall indication of specificity and indicates that **3** is a narrow-spectrum kinase inhibitor.

IC$_{50}$ of **1 – 6** Against Relevant Kinases

Based on the kinase inhibition profiling of **3** and **4**, 13 kinases were selected for determination of IC$_{50}$ values against **2 – 6** (Table 4). As **1** did not significantly inhibit any of the kinases at 50 µM, it was not included in the IC$_{50}$ determination. PIM2 and Aurora B were included to highlight the selectivity of inhibition of the closely related kinases PIM1 and PIM3[28] and Aurora A[29], respectively. The difference in the kinase inhibition potency of **1 – 6** correlated well with the cancer cell cytotoxic data (MTS assay) recorded for the same compounds. Although we have not observed a functional correlation of the inhibition of a specific or single kinase with antiproliferative activity yet, breitfussin analogs inhibiting multiple kinases *in vitro* have higher potency in the cytotoxicity assays. This is beyond this initial characterization of the breitfussins as kinase inhibitors and it is going to be the task of future optimization chemistry to generate highly selective analogs from the breitfussin scaffold, which are expected to show a clear functional correlation *in vitro* and in functional cellular assays. Compound **3** was the most potent inhibitor, giving IC$_{50}$ values as low as 200 nM ± 50 (PIM1). Based on the results from the *in vitro* cancer cell cytotoxic and kinase inhibition profiles of **1 – 6**, **3** was selected for further studies to evaluate the pharmacological potential of the breitfussin scaffold.

Table 4. IC_{50} determination of **2 – 6** against 13 kinases nominated through kinase profiling of **3** and **4**.

Kinase	Compound IC_{50} (µM)					
	1	**2**	**3**	**4**	**5**	**6**
DYRK1A	na[a]	na	2.3 ±0.2	na	na	na
ERK8	na	na	1.0 ±0.1	46 ±7	na	na
PIM1	na	na	0.2 ±0.05	0.9 ±0.01	43 ±12	18 ±9
PIM2	na	na	11 ±2	22 ±3	na	na
PIM3	na	na	1.8 ±0.1	3.7 ±0.8	na	na
SIK3	na	na	1.2 ±0.1	na	na	na
GCK	na	na	0.6 ±0.06	1.2 ±0.1	na	40 ±5
TAK1	na	na	1.2 ±0.1	1.0 ±0.1	36 ±15	18 ±7
MLK1	na	na	0.6 ±0.12	0.9 ±0.04	22 ±2	21 ±7
MLK3	na	na	0.6 ±0.05	0.5 ±0.05	23 ±2	19 ±2
RIPK2	na	na	1.1 ±0.2	na	na	na
Aurora A	na	na	22 ±6	na	na	na
Aurora B	na	na	0.8 ±0.02	0.9 ±0.23	7.8 ±0.2	31 ±3

[a]Not active (IC_{50} > 50 µM)

Extended Kinase Inhibition Profile for **3**

The binding affinities of **3** were tested at 10 µM against 468 kinases and pseudo kinases found in the DiscoverX ScanMax panel (Figure 4, Table S4). In these active-site directed competition binding assays, a kinase ligand is immobilized to a solid support. The amount of kinase bound to the immobilized ligand in the presence and absence (control) of **3** were quantified, and the affinity of **3** to the kinase active site was reported as percent of control (PoC).[30, 31] At 10 µM, **3** gave PoC values lower than 35% for 30 kinases. The strongest affinity of **3** was observed against the three

related Ca^{2+}/calmodulin-dependent protein kinases MYLK4, DRAK2 and DRAK1, with PoC values of 0.25, 1.2 and 2.9%, respectively. PIM1, the kinase against which the lowest IC_{50} value for **3** was measured in the ICKP activity assay (IC_{50} = 0.2 µM), gave a PoC of 9.5%. Compound **3** had stronger affinity towards PIM1 than PIM2 and PIM3 (PoC: PIM3 = 21%, PIM2 = 54%). The relative affinities of the PIM kinases correlated well with the IC_{50} values found in the activity assays (IC_{50}: PIM3 = 1.8 µM, PIM2 = 11 µM).
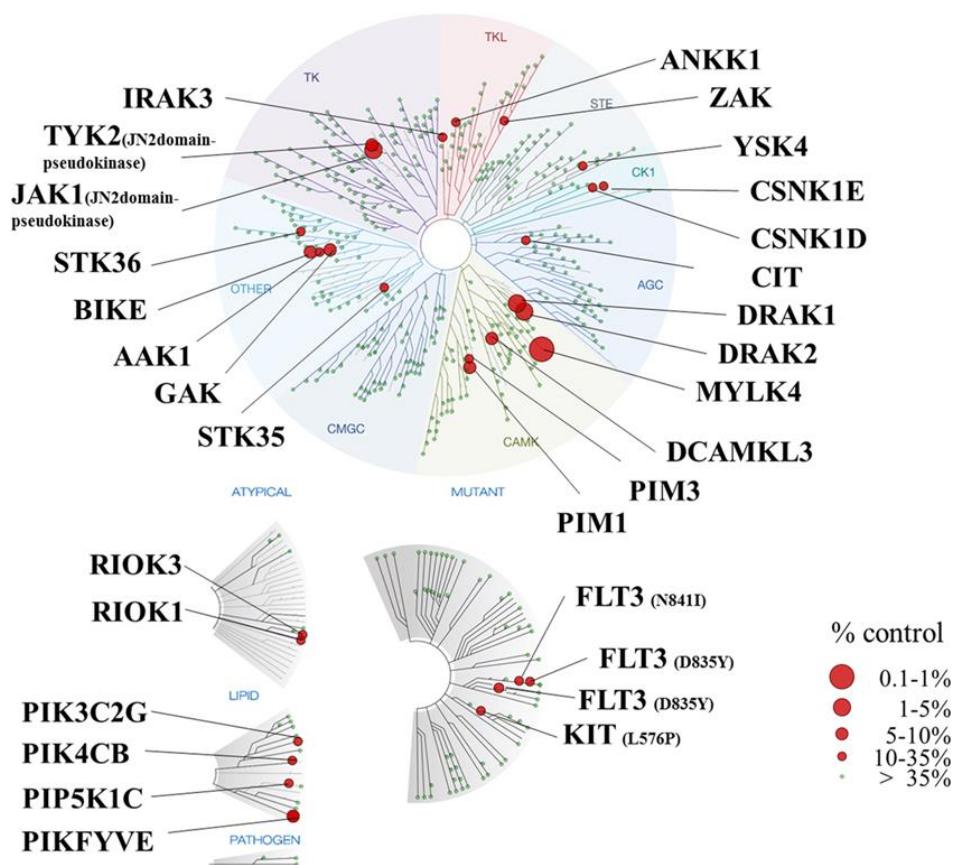

Figure 4. Kinome binding affinity data of compound **3** at 10 µM against 468 kinases. The disc sizes encode the level of residual activity as shown in the figure key.

Furthermore, the K_d values of **3** against the 19 kinases with lowest PoC values were determined (Table 5). When comparing the results obtained for **3** from the ICKP and the DiscoverX panels,

two kinases were found to be among the most sensitive candidates in both assays: PIM1 and PIM3 (PIM1: IC_{50} = 200 nM, K_d = 1.2 µM and PIM3: IC_{50}= 1.79 µM, K_d = 4.7 µM). All the 11 remaining kinases, for which IC_{50} values were determined at ICKP, were tested at 10 µM at DiscoverX, however, **3** did not bind strong enough to these for K_d determination to be prioritized (PoC at 10 µM: DYRK1A: 75%, ERK8: 67%; SIK3 (QSK in DiscoverX panel): 94%; GCK (MAP4K2 in DiscoverX panel): 72%; TAK1: 70%; MLK1: 59%; MLK3: 56%; Pim2: 54%; RIPK2: 57%; AuroraA: 80%; AuroraB: 50%). The remaining enzymes against which the K_d values of **3** were determined in the DiscoverX panel, were not available in the ICKP panel. Disagreement between binding- and activity based assays are not uncommon and can be explained by the use of different constructs, expression systems, purification protocols and assay conditions.[32] The affinity of **3** towards kinases and the selective nature of this interaction, was however confirmed through the data obtained from DiscoverX.

Table 5. K_d values of **3** against the DiscoverX kinases with strongest binding affinities.

Kinase	K_d (µM)	Kinase	K_d (µM)	Kinase	K_d (µM)
DRAK2	0.39 ±0.04	STK35	1.3 ±0.1	DRAK1	2.8 ±1.3
MYLK4	0.43 ±0.07	IRAK3	1.7 ±0.2	PIK4CB	2.9 ±0.3
GAK	0.44 ±0.02	TYK2*	1.8 ±0.1	RIOK1	2.9 ±1.8
JAK1*	1.0 ±0.1	DCAMKL3	1.8 ±0.2	CSNK1E	3.3 ±0.2
PIKFYVE	1.0 ±0.1	CIT	2.7 ±0.1	PIM3	4.7 ±0.3
BIKE	1.1 ±0.1	STK36	2.7 ±0.1	FLT3 (N841I mutant)	8.9 ±4.2
PIM1	1.2 ±0.3				

*JH2domain-pseudokinase

Several of the kinases inhibited by or binding to **3** are validated as anticancer targets. To name a few, the PIM kinases are known drivers in many cancers, including triple negative breast cancer.[33] Mutants of FLT3 kinase occur in approximately 30% of all acute myeloid leukemia cases[34] and ERK8 and AuroraB are highly expressed in several human cancers, including lung cancer.[35, 36] The exact cellular target(s) responsible for the observed cytotoxic activities of **3** remain to be determined and may be due to pan-kinase inhibition.

Selective Cytotoxic Activity of **3**

To get more information on the selectivity of **3** against a broader panel of cell lines, IC_{50} values of **3** were determined against 88 cancer cell lines and proliferating peripheral blood mononuclear cells (PBMCs) in the OncoLead cell panel using a sulforhodamine B protein staining assay technique (Figure 5 and Table S6).[37] The cell lines included in this panel covers multiple cancer types (overview in figure 5) and the IC_{50} values against the 10 most affected cell lines are listed in Table 6. The results from this screening confirmed the potent and selective cytotoxic activity of **3** with activities at low μM/sub-μM IC_{50} concentrations (lowest $IC_{50} = 0.34$ μM). In comparison, the lowest reported IC_{50} value of the kinase inhibitor roscovitine, which is currently under clinical development as an anticancer agent, was 4.9 μM in a comparable assay setup.[38] In total, 48 out of the 88 cell lines were affected to some extent by exposure to **3**. The most striking results from these experiments are the ability to specifically inhibit the viability of selected breast cancer cell lines. Most potently inhibited cell line was the drug-resistant triple negative breast cancer (TNBC) cell line MDA-MB-468 ($IC_{50} = 340$ nM). In our in-house MTS based cancer cell cytotoxic assay the MDA-MB-468 cell line was significantly less affected (IC_{50} value > 10 μM). While the MTS assay is considered a precise and specific *in vitro* assay

for measuring cytotoxic activity of investigated agents, it has been shown that colorimetric assays may underestimate anti-proliferative effects.[39] For example, damaged mitochondria may still be able to reduce the dye and investigated agents may interfere with mitochondrial dehydrogenase activity.[40, 41] This discrepancy is thus most likely due to the difference in assay technique. The following breast cancer cell lines were also affected: MCF-7 (IC_{50} = 0.77 µM), MT3 (IC_{50} = 0.93 µM), SK-BR-3 (IC_{50} = 1.53 µM), JIMT1 (IC_{50} = 4.17) and the TNBC cell line HS578T (IC_{50} = 5.22 µM).
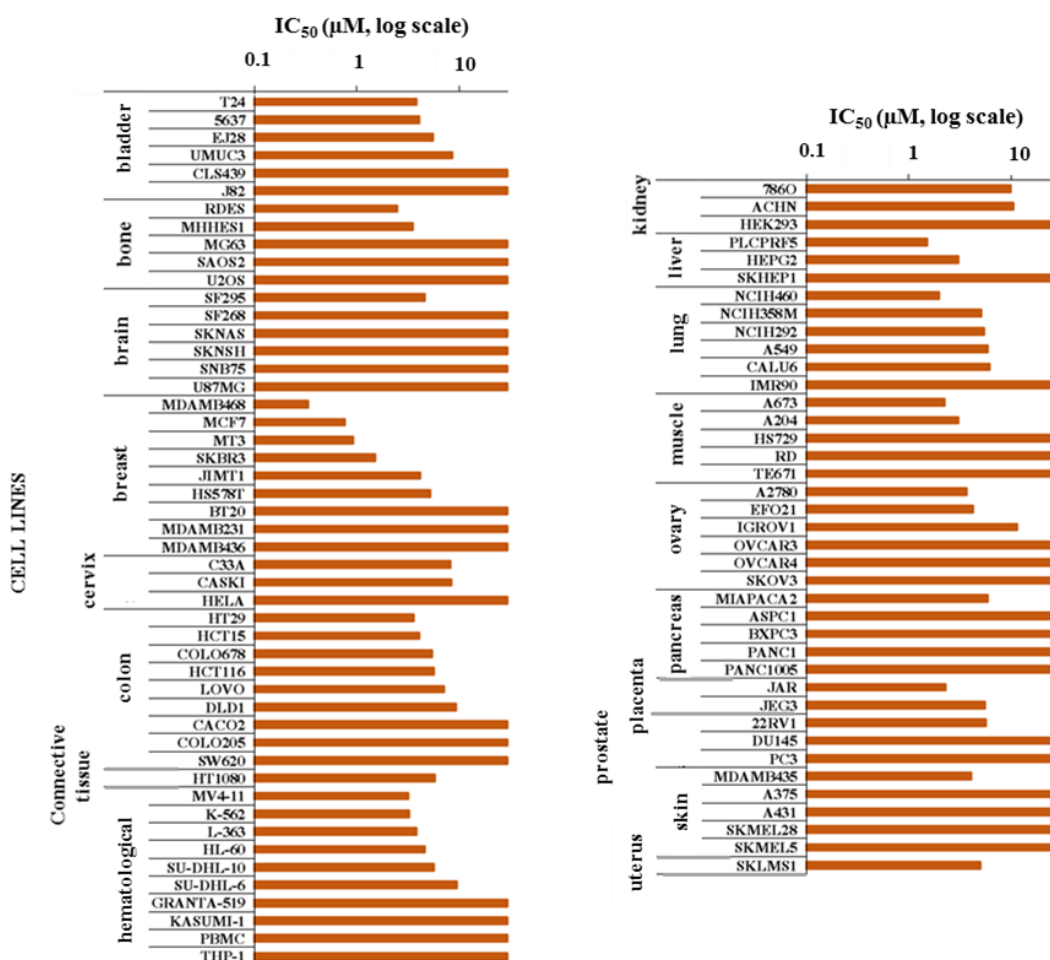

Figure 5. IC_{50} values for **3** against the 88 cell lines found in the OncoLead panel (Z-scores in Table S8)

Table 6. The 10 cancer cell lines in the OncoLead panel that were most affected by **3**.

Cell line	Origin	IC$_{50}$ (µM)	Z-score
MDA-MB-468	Breast	0.34	-3.87
MCF-7	Breast	0.77	-2.47
MT3	Breast	0.93	-2.35
PLCPRF5	Liver	1.5	-1.6
SK-BR-3	Breast	1.5	1.1
NCIH460	Lung	2.0	-1.0
A673	Muscle	2.2	-1.0
JAR	Placenta	2.3	-0.8
RDES	Bone	2.5	-0.9
HEPG2	Liver	3.0	-0.6

Compound **3** had no or significantly lower effect against the remaining breast cancer cell lines: BT20, MDA-MB-231 and MDA-MB-436 (IC$_{50}$ values > 30 µM). The non-malignant human PBMCs and 39 cancer cell lines were not affected even at the highest dose of 30 µM of **3**.

Such a differential inhibition profile in a broad cancer cell panel is typically observed when one or a few molecular mechanisms of inhibition are present in the sensitive cell lines. Therefore, it is our assumption that **3** inhibits one or a few proliferation relevant kinases, which are important drivers of cancer formation.

Natural product often serve as lead templates that are subjected to structural optimization to generate clinically useful structures.[42] Selective and potent activity against cancer cells (IC$_{50}$ values < 1 µM) and inhibition of kinases in the nM range show the value of the breitfussin scaffold as an excellent starting point for the development of an anticancer compound. In comparison, rohitukine, a flavonoid alkaloid initially isolated *Amoora rohituka*, gave IC$_{50}$ values of 300 ± 15 nM against

the kinase CDK-9 and GI$_{50}$ values of 10 – 28 µM against five cancer cell lines.[43] Medicinal chemistry efforts based on the rohitukine scaffold rewarded two new promising clinical candidates, flavopiridol and riviciclib.[44] Both are currently undergoing clinical evaluation as anticancer agents targeting several kinases where the primary mechanism of action is believed to be through CDK-9 inhibition.[44] Riviciclib has an IC$_{50}$ value of 20 nM against CDK-9.[43]

Mode-of-Action of the Breitfussins against the Kinases

Many natural product kinase inhibitors or derivatives thereof, like roscovitine, as well as synthetic small molecule kinase inhibitors inhibit their targets by competition with ATP.[7, 8] The ICKP and DiscoverX assay technologies are biased towards ATP competitiveness as mode-of-action. We therefore tested the ability of **1** - **4** to bind to the ATP binding pocket employing two different tracer displacement assays. As the assays herein used to measure ATP competitiveness are based on binding affinity, DRAK2 and DRAK1, to kinases with closely related structures,[45] were chosen as model kinases at they display strong binding affinity towards **3** (K$_d$ (µM): DRAK2 = 0.39 ±0.04, DRAK1 = 2.8 ±1.3).

The cell free ATP-competitive tracer displacement assays[46] are based on the binding and displacement of the Alexa Fluor 647-labelled ATP competitive kinase tracer to glutathione S-transferase (GST)-tagged DRAK1 and DRAK2. Tracer binding was detected by using europium (Eu)-labelled anti-GST antibodies. Simultaneous binding of both fluorescent tracer and antibody to the GST-tagged kinase generated a fluorescence resonance energy transfer (FRET) signal. When adding an inhibitor, which competes with binding of the tracer, a loss of the FRET signal was observed. Using this assay, **3** and **4** were shown to bind to the ATP binding pocket (Table 7). To evaluate the binding of **1** – **4** to the ATP binding site within living permeabilized cells (cells

permeabilized using digitonin), the NanoBRET kinase target engagement assay was used.[47] This target engagement assay is based on an energy transfer technique designed to measure molecular proximity in living cells and cell lysates. This intracellular kinase assay measures the apparent affinity of test compounds by competitive displacement of a tracer molecule reversibly bound to the ATP binding site of a kinase fused with the NanoLuc luciferase. In the first step of this assay, a fixed concentration of tracer was added to cells expressing the desired NanoLuc fusion protein to generate a BRET reporter complex. Introduction of competing compounds results in a dose-dependent decrease in NanoBRET energy transfer allowing for quantitation of the intracellular affinity of the target protein for the test compound. In this assay, **2** - **4** were shown to bind to the ATP binding pocket of DRAK1 and DRAK2 (Table 7).

Table 7. The ATP competitiveness of compounds **1** – **4**.

	IC_{50} (µM)	
	DRAK1	DRAK2
Comp.	Cell free tracer displacement assay	
1	>10	>10
2	>10	>10
3	4.6	9.8
4	9.6	>10
	Intracellular tracer displacement assay	
1	>10	>10
2	>10	3.3
3	3.0	0.5
4	>10	8.3

In both assay formats, selected breitfussins were shown to bind to the ATP binding site of the selected kinases by displacing the tracers from the ATP binding sites of DRAK1 and DRAK2.

Docking of **3** to the ATP-binding pocket of PIM1

To complete the scenario of identifying the ATP binding pocket as the site of interaction between **3** and the kinases, **3** was docked manually and computationally using Glide into a cocrystal structure of PIM1 (Protein Data Bank access code 4K1B) (Figure 6). Several binding modes were obtained, submitted to a short molecular dynamics run, and minimized. The pyrrole and indole N-H groups are complementary to the two C=O groups available as hydrogen bond acceptors in the hinge region of PIM1. The pyrrole and indole N-H groups form hydrogen bonds to the hinge backbone C=O groups of Pro123 and Glu121. The indole is stacked between lipophilic residues and does not interfere with the gate keeper residue (Leu120). Through this experiment, we were able to determine binding to the ATP-binding pocket as mode-of-action for **3**.
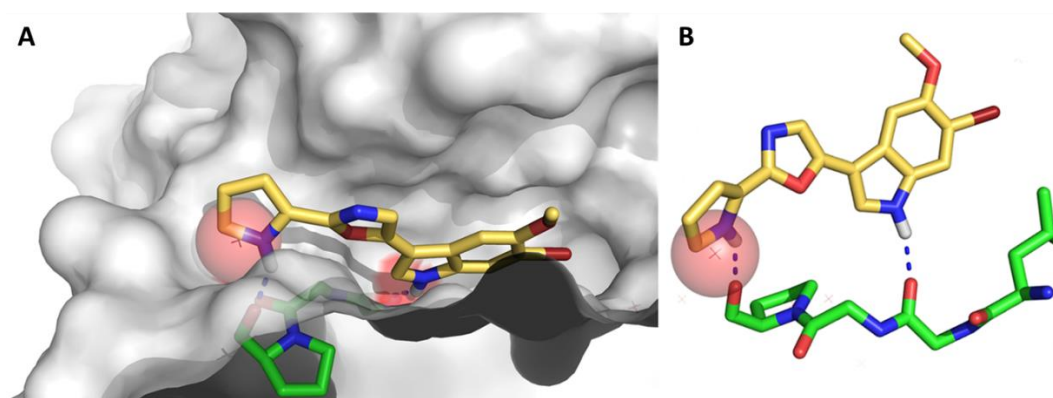

Figure 6. Binding mode of **3** with the ATP-binding pocket of PIM1 (PDB: 4K1B). Compound **3** is shown with yellow carbon atoms, the hinge backbone carbon atoms of PIM1 are in green (Pro123, Arg122, Glu121, Leu120). A water molecule present in 4K1B is replaced by the pyrrole and is shown as a red sphere. A: Surface representation of the ATP-binding pocket of PIM1 with compound **3**. B: Detailed view of the interaction between the PIM1 hinge residues and **3**.

Potential Off-Target Effects of **3**

To evaluate potential off-targets interactions for **3**, a diversity panel screen at 10 µM was performed using the Cerep Panlabs diversity panel (previous version now known as the Eurofins discovery safetyscreen panel). The panel was designed to assess potential adverse effects of a lead compound. In total, only 16 out of 98 targets were affected to the point where percentage inhibition of control values (phosphodiesterase type 4D2 and phosphodiesterase type 5, Figure 7) and specific binding (rest) were defined as active (above 50%). The remaining 82 targets were below 50% (Table S5A and B). On the list of affected targets, the majority were receptors. In addition, a transporter (norepinephrine transporter) and two enzymes (phosphodiesterase type 4D2 and 5) were also affected. As most of the targets will not affected at concentrations corresponding to the IC_{50} or K_d values for the on-target effects, **3** is considered as having promising selectivity.
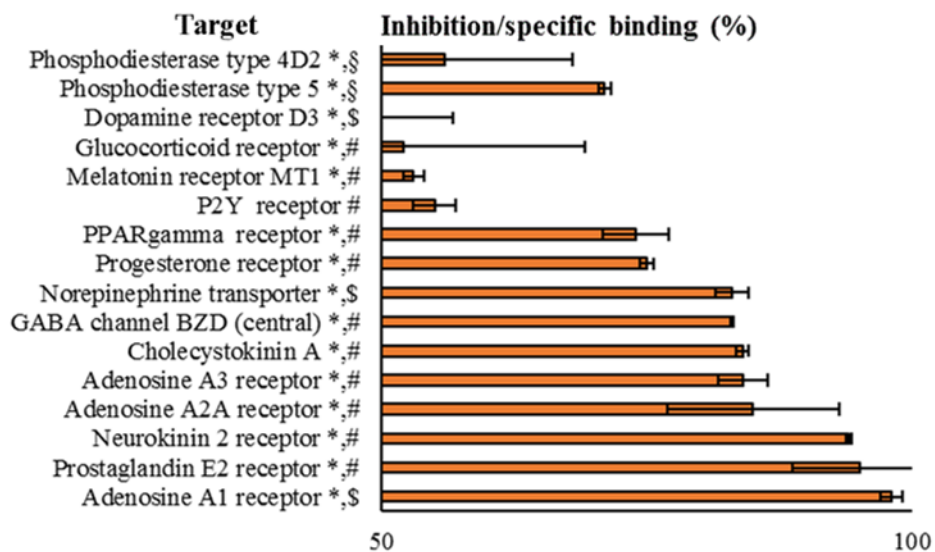

Figure 7. Potential off-targets (>50%) of **3** tested at 10 µM in the Cerep Panlabs diversity profile panel. *=human, #=agonist, $=antagonist, §=enzymatic assay

In vivo Toxicity of **3**

The toxicity of **3** against zebrafish embryos was evaluated by recording survival and toxic phenotype formations, including cardiac edema, scoliosis, tail degeneration, necrosis and generalized edema. The assay was conducted at the BioReperia laboratory. Zebrafish embryos are considered a powerful tool to assess toxicity as it allows for whole-animal investigation.[48] At 72 h exposure, the concentration resulting in 50% lethality (LD_{50}) was 1.4 μM. This value is four-fold higher than the most potently inhibited cell line in the OncoLead panel. Toxic phenotypes were only evaluated on living embryos, and the results are given as the percent of embryos not exhibiting the toxic phenotype (Figure 8 and Table 8).
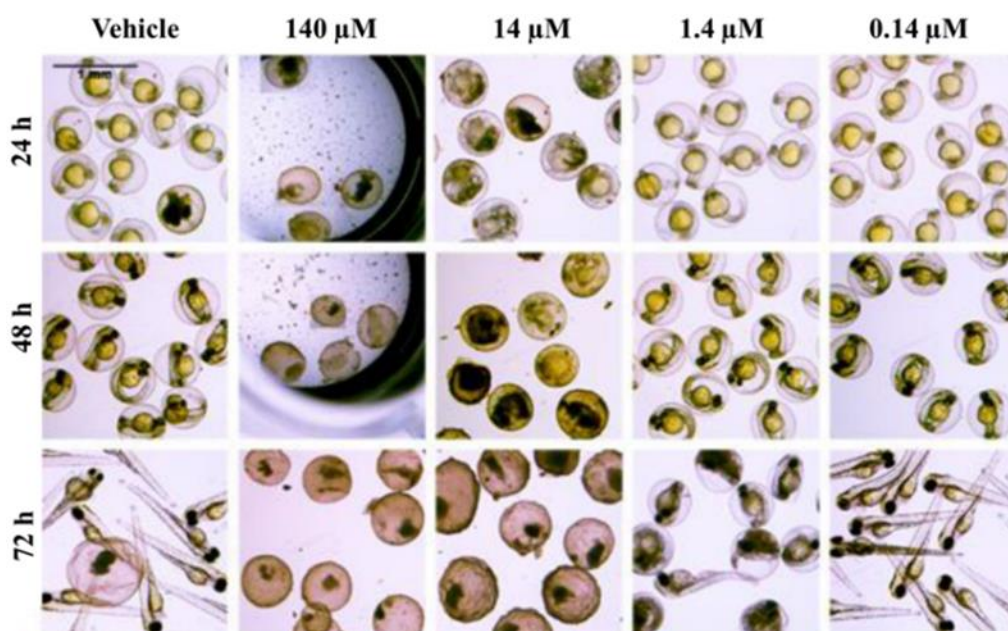

Figure 8. Assessment of toxicity of **3** against zebrafish embryos.

Table 8. Embryos being healthy and not exhibiting the indicated issues of toxicity or death, expressed as % of all living embryos after being exposed to **3** for 72h.

	Unaffected embryos (%)					
Conc. (µM):	1396	140	14	1.4	0.1	0
Toxicological issue						
Survival	0,0	0,0	5	45	100	95
Heart edema	NA[a]	NA	100	100	95	100
Scoliosis	NA	NA	0	89	95	100
Tail degeneration	NA	NA	0	100	100	100
Necrosis	NA	NA	0	0	100	100
General edema	NA	NA	100	100	100	100

[a]NA: Not available

In general, heart edema and generalized edema were not observed to any significant degree in response to any non-lethal concentration of **3**. Scoliosis and tail degeneration were observed in all embryos exposed to the highest non-lethal concentration of **3** (1.4 µM). Compound **3** was poorly soluble in the assay media (PTU-E3 water). Precipitated **3** was evident for the highest test concentrations (1396 (data not shown in Figure 8), 140 and 14 µM).

Determination of *In Vitro* ADME Parameters of **3**

Compound **3** was profiled in an *in vitro* ADME assay panel to address its aqueous kinetic solubility, permeability through artificial membranes (PAMPA), metabolic stability under oxidative and conjugative conditions, plasma stability and degree of plasma protein binding (Table 9).

Table 9. *In vitro* ADME parameters of **3**.

Assay	Output	
Human MS[a] phase I Cl_{int}	14	µL/min/mg
Mouse MS phase I Cl_{int}	47	µL/min/mg
Human MS phase II	92	% remaining after 1 h at 5 µM
Mouse MS phase II	100	% remaining after 1 h at 5 µM
Membrane permeability	23	Flux [%]
Human plasma protein binding	0.3	% unbound at 5 µM
Mouse plasma protein binding	0.3	% unbound at 5 µM
Human Plasma Stability	83	% remaining after 1 h at 5 µM
Mouse Plasma Stability	84	% remaining after 1 h at 5 µM
Solubility at pH 7.4	156	µM

[a]MS: Microsomal stability

In all these assays, **3** was found to have favorable properties as a lead compound. Particularly, the moderate intrinsic clearance (Cl_{int}) value of 47 µL/min/mg obtained in the presence of mouse liver microsomes and the acceptable stability of 85% in mouse plasma predicts good exposure in mice. Mice will thus be a suited species for proof-of-concept studies in the future. In this regard, it will be interesting to determine the pharmacokinetic parameters in mice as a next step to see how well the *in vitro* profile correlates with the *in vivo* ADME properties.

CONCLUSION

The results from this investigation into the cytotoxic activities, kinase inhibition and ADME and toxicological properties of the breitfussins (**3** in particular) clearly show the potential of the breitfussin scaffold for further development of lead compounds primarily with antiproliferative

activity. Even as non-modified natural products, the breitfussins show preferential binding to kinases and inhibition of cell viability at promising potency and selectivity. We consider the breitfussin to be an interesting scaffold of narrow-spectrum kinase inhibitors. Further exploration of the series might quickly lead to the generation of more selective inhibitors of the indicated kinase subfamilies.

EXPERIMENTAL SECTION

Materials and methods for natural product isolation and structure elucidation

General experimental procedures

A Waters 600 Pump monitored by a 2996 Photodiode Array UV detector and a 3100 single quadrupole MS were used for mass guided preparative HPLC over a Waters XSelect CSHTM Prep Fluoro-Phenyl column (5 μm 10*250 mm). A Waters LCT Premier Time-of-Flight mass spectrometer with a Waters Acquity UPLC was used for acquisition of high-resolution mass data. The purity of key compounds (isolated **3** and **4** and synthetically produced **3**) were measured using UHPLC-UV analysis and calculated using the UV purity tool in the Waters UNIFY Scientific Information System software. The purity was determined to be ≥95% for all key compounds.

Reagents and materials

HPLC grade acetonitrile (ACN) and methanol (MeOH) (Chromasolve®, for preparative HPLC), LC-MS grade ACN (Chromasolve®, for LC-MS analysis) and reagent-grade formic acid (≥98%) were purchased from Sigma- Aldrich (Steinheim, Germany). Ultra-pure water was prepared using a Millipore Milli-Q purification system (Bedford, MA, USA). Deuterated DMSO and methanol were purchased from Sigma-Aldrich (Steinheim, Germany). Roswell Park Memorial Institute (RPMI, Merck KGaA), Earle's minimal essential medium (E-MEM, Merck, Germany),

Dulbecco's modified Eagle's medium (D-MEM, Thermo Fisher Scientific), McCoy's 5A (Biowest, France), Leibovitz L15 Medium (L15, Biowest, France) and Iscove Basal Medium with stable glutamine (Merck, Germany) cell media were used. D-MEM and RPMI were supplied with 10% fetal bovine serum (FBS, Merck) and 5 mL L-alanyl-L-glutamine (200 mM, Merck, Germany). E-MEM was supplied with 10% FBS, 5 mL L-alanyl-L-glutamine, 5mL non-essential amino acids (100x, Merck, Germany), 5 mL sodium pyruvate (100 mM, Merck, Germany) and 5 mL sodium bicarbonate (7.5%, Merck, Germany). McCoy's 5A and Iscove basal medium were supplied with 10% FBS. L15 was supplied with 10% FBS and 5 mL sodium bicarbonate. All media were supplied with gentamycin (10 µg/mL, Merck, Germany).

Biomass collection

Specimens of the cnidarian *Thuiaria breitfussi* (class Hydrozoa, order Leptothecata, family Sertulariidae) were collected with a triangular bottom scrape in September 2011 at Bjørnøya, Svalbard (79.0293 N, 20.8574 E, at 48 m depth). The organism was identified by Robert A. Johansen, the Norwegian national biobank (Marbank) and a voucher specimen (reference number: M13031) was deposited at Marbank, Tromsø, Norway.

Isolation of breitfussin A – H (1 – 8)

The frozen specimens of *T. breitfussi* (475.6 g) were freeze-dried and minced. The resulting mass (96.6 g) was extracted twice with water (24 h and 30 min, respectively) at 5 °C in the dark. After centrifugation the remaining sediment was freeze-dried, minced, and extracted twice with a 1:1 (vol:vol) mixture of dichloromethane and MeOH and filtrated. The filtrate was dried, resulting in 6.0 g organic extract. An aliquot of the organic extract (4.3 g) was partitioned between 150 mL hexane and 150 mL 90% MeOH three times to remove very lipophilic compounds. The pooled

MeOH fractions were dried under reduced pressure and redissolved in 13 mL MeOH. Aliquots of this solution were injected onto a fluoro-phenyl column (gradient of 45 to 65% of ACN (aq) over 20 min, 6 mL/min). In the end, eight breitfussins were isolated in amounts that enabled structure determination by NMR. Out of these, six were pure compounds: **1** (4.2 mg), **2** (3.1 mg), **3** (7.3 mg), **4** (2.2 mg), **5** (2.0 mg), **6** (1.9 mg). We were not able to separate **7** and **8**, and a mixture of the two (1.33 mg in total) was submitted to NMR analysis.

NMR analysis of isolated 3 - 8

All NMR data were acquired on a Varian/Agilent Inova spectrometer operating at 599.934 and 150.863 MHz for ^{1}H and ^{13}C respectively, using a cryogenically cooled inverse detection HCN probe with enhanced proton channel (2nd generation). All spectra were acquired at 298 K in DMSO-d_6. Data acquired in DMSO-d_6 was referred to the residual solvent peak of DMSO-d_6, ^{1}H = 2.504 and ^{13}C = 39.98 ppm. Typically, 16-32k data points were acquired for the 1D 1H experiments using 90° reading pulses, 5 seconds relaxation delay and 8-32 transients. For the 2D phase insensitive gradient selected COSY experiments, 1440 x 200 complex data points were acquired using 4-8 transients. Data matrices of 1440 x 200 and 1440 x 256 complex points were acquired for the gradient selected edited HSQC and absolute value HMBC respectively, using 8 to 32 transients. ROESY spectra were acquired as 1440 x 256 complex data points and 8 transients, with spinlock duration of 300 ms at 36 dB. For carbon 1D spectra, 32k complex data points were acquired, using 45-90° reading pulses, 1-5 seconds relaxation delay and 10000-20000 transients applying 1H decoupling during both relaxation and acquisition time. All spectra were acquired at 298 K in both DMSO-d_6 (Sigma-Aldrich) and methanol-d_4 (Sigma-Aldrich) using sweep widths of 9600 and 30200-37800 Hz for ^{1}H and ^{13}C, respectively. Two-dimensional experiments were acquired using the grad-90-grad option with 2 ms homospoil gradient time at 5796 Hz. Data

acquired in DMSO-d_6 was referenced to the residual solvent peak of DMSO-d_6, ^{1}H = 2.504 and ^{13}C = 39.98 ppm.

Synthesis of 3 and 4

General

All reactants, reagents and solvents were purchased from Sigma-Aldrich and used as delivered unless otherwise stated. Compound **19** was prepared as previously described.[10] Moisture sensitive reactions were carried out under an argon atmosphere in oven-dried (130 °C) equipment that had been cooled down under vacuum. Solvents used for moisture sensitive reactions were obtained from an anhydrous solvent delivery system (SPS-800 system from M. Braun GmbH, Garching, Germany). Anhydrous THF was obtained from the SPS-800 or from a sodium/benzophenone still. Flash chromatography was performed using silica gel from Merck (Silica gel 60, 0.040 – 0.063 mm) or Grace GmbH (35-70 micron). TLC analyses were performed on aluminium sheets coated with Merck TLC silica gel 60 F254 and visualization was achieved by using ultraviolet light (254 nm) or a solution of phosphormolybdic acid in ethanol. The NMR-experiments were recorded on a Bruker Ascend 400 or a Bruker BioSpin AV500 at ambient temperature. ^{1}H and ^{13}C chemical shifts (δ) are reported in ppm with reference to the solvent residue peak (CDCl$_3$: δ_H = 7.26 and δ_C = 77.16; DMSO-d_6: δ_H = 2.50 and δ_C = 39.98). All coupling constants are given in Hz. ESI-HRMS was conducted on a Thermo electron LTQ Orbitrap XL spectrometer (Thermos, Bremen, Germany) with methanol as solvent.

5-(6-Bromo-5-methoxy-1*H*-indol-3-yl)-2-(1*H*-pyrrol-2-yl)oxazole (3, breifussin C)

A solution of **18** (70 mg, 0.095 mmol) in anhydrous CH_2Cl_2 (0.7 mL) was cooled to 0 °C and treated with TFA (0.7 mL). The resulting mixture was stirred at rt overnight before it was concentrated under reduced pressure and separated between water (5 mL) and EtOAc (5 mL). The organic layer was washed with and saturated NaCl (3 mL), dried over $MgSO_4$, and concentrated under reduced pressure. The resulting material was dissolved in anhydrous THF (1.0 mL) and cooled to 0 °C before it was treated with TBAF (104 µL, 1M in THF, 104 µmol). The resulting mixture was stirred for 20 min at 0 °C before saturated NH_4Cl (5 mL) was added. The resulting mixture was extracted with EtOAc (2 × 5 mL) and the combined organic layers were washed with saturated NaCl (5 mL) and dried over $MgSO_4$. After removal of the solvent under reduced pressure, the crude product was purified by flash chromatography (hexane/EtOAc, 7:3 v/v to 2:3 v/v) to give the title compound **3** (23 mg, 68%) as a colorless solid. R_f (hexanes/EtOAc, 1:1 v/v) = 0.25; ^1H NMR (500 MHz, (DMSO-d_6): δ = 11.84 (s, 1H), 11.52 (d, J = 2.7 Hz, 1H), 7.82 (d, J = 2.5 Hz, 1H), 7.70 (s, 1H), 7.54 (s, 1H), 7.43 (s, 1H), 6.98 (q, J = 2.2 Hz, 1H), 6.76 (q, J = 1.9 Hz, 1H), 6.22 (dd, J = 3.8, 1.9 Hz, 1H), 3.96 (s, 3H); ^{13}C NMR (126 MHz, (DMSO-d_6): δ = 154.6, 150.5, 146.0, 132.0, 124.8, 123.7, 122.1, 120.7, 120.5, 116.6, 109.8 (2C), 107.2, 104.4, 102.3, 57.1.

5-(6-Bromo-4-methoxy-1*H*-indol-3-yl)-2-(1*H*-pyrrol-2-yl)oxazole (4, breitfussin D)

A solution of **19** (51 mg, 69 µmol) in anhydrous CH_2Cl_2 (0.5 mL) was cooled to 0 °C and treated with TFA (0.5 mL). The resulting mixture was stirred at rt overnight before it was concentrated under reduced pressure and separated between water (3 mL) and EtOAc (3 mL). The organic layer was washed with saturated NaCl (3 mL), dried over $MgSO_4$, and concentrated under reduced pressure. The resulting material was dissolved in anhydrous THF (0.7 mL) and cooled to 0 °C

before it was treated with TBAF (72 µL, 1M in THF, 72 µmol). The resulting mixture was stirred for 20 min at 0 °C before saturated NH$_4$Cl (4 mL) was added. The resulting mixture was extracted with EtOAc (2 × 4 mL) and the combined organic layers were washed with saturated NaCl (3 mL) and dried over MgSO$_4$. After removal of the solvent under reduced pressure, the crude product was purified by flash chromatography (hexane/EtOAc, 7:3 v/v to 2:3 v/v) to give the title compound **4** (19 mg, 77%) as a colorless solid. R$_f$ (hexanes/EtOAc, 1:1 v/v) = 0.25; ^{1}H NMR (400 MHz, (DMSO-d_6) δ = 11.80 (s, 1H), 11.71 (s, 1H), 7.74 (s, 1H), 7.35 (d, J = 2.8 Hz, 1H), 7.25 (d, J = 2.4 Hz, 1H), 6.97 (s, 1H), 6.73 (br. s, 2H), 6.23 – 6.18 (m, 1H), 3.95 (s, 3H); ^{13}C NMR (101 MHz, (DMSO-d_6): δ = 154.7, 154.1, 146.2, 139.0, 123.8, 123.2, 122.0, 120.5, 115.8, 113.2, 109.8 (2C), 108.5, 104.6, 104.4, 56.0.; HRMS (ESI): m/z [M+H]$^+$ calcd for C$_{16}$H$_{13}$BrIN$_3$O$_2$$^+$: 358. 0186 and 360.0165; found: 358. 0186 and 360.0164.

5-Methoxy-1-(triisopropylsilyl)-1*H*-indole (10)

A solution of 5-methoxyindole (1.997 g, 13.57 mmol) in dry THF (16 mL) was added to a suspension of sodium hydride (843 mg, 60% w/w in mineral oil, 21.1 mmol) in THF (14 mL) at 0 °C, and the resulting mixture was stirred at 0 °C for 1 h before TIPSCl (1.6 mL, 72.5 mmol) was added. The mixture was warmed to room temperature and stirred overnight (22 h), before saturated NH$_4$Cl (60 mL) was added. The resulting mixture was extracted with Et$_2$O (3 x 70 mL) and the combined organic layers were dried over MgSO$_4$. After filtration and removal of the solvent *in vacuo*, the crude product was purified using flash chromatography (petroleum ether/toluene, 6:1 v/v) to give the title compound **10** (3.818 g, 93%) as a transparent oil. ^{1}H NMR (400 MHz, CDCl$_3$): δ = 7.40 (dd, J = 9.0, 0.8 Hz, 1H), 7.23 (d, J = 3.2 Hz, 1H), 7.10 (d, J = 2.6 Hz, 1H), 6.81 (dd, J = 9.0, 2.6 Hz, 1H), 6.56 (dd, J = 3.1, 0.8 Hz, 1H), 3.86 (s, 3H), 1.67 (sept, J = 7.5 Hz, 3H), 1.14 (d,

J = 7.5 Hz, 18H); ^{13}C NMR (100 MHz, CDCl$_3$): δ = 154.1, 135.9, 132.1, 132.0 (2C), 114.6, 111.4, 104.6, 102.3, 55.8, 18.3, 12.9. The analytical data were in accordance with those reported in the literature.[17]

6-Bromo-5-methoxy-1-(triisopropylsilyl)-1*H*-indole (11)

To a solution of **10** (2.811 g, 9.26 mmol) and TMEDA (1.67 mL, 11.14 mmol) in dry THF (45 mL) was added *sec*-butyl lithium (9.10, 11.10 mmol) dropwise over 20 min at -15 to -5 °C. The mixture was stirred for an additional 20 min at -5 °C before 1,2-dibromoethane (1.0 mL, 11.60 mmol) was added. The resulting mixture was warmed to room temperature and stirred for 45 min before saturated NH$_4$Cl (70 mL) was added and the resulting mixture was extracted with Et$_2$O (3 x 100 mL). The combined organic layers were dried over MgSO$_4$, filtered and concentrated *in vacuo*. The crude product was purified using flash chromatography (petroleum ether/toluene, 6:1 v/v) to give a 2:3 mixture (2.363 g, 67%) of **11** and **12**, from which the title compound **12** could be isolated as a colorless solid (496 mg, 14%) by crystallization from hexane. ^{1}H NMR (400 MHz, CDCl$_3$): δ = 7.66 (d, J = 0.9 Hz, 1H), 7.21 (d, J = 3.2 Hz, 1H), 7.12 (s, 1H), 6.54 (dd, J = 3.1, 0.9 Hz, 1H), 3.92 (s, 3H), 1.65 (sept, J = 7.5 Hz, 3H), 1.14 (d, J = 7.5 Hz, 18H); ^{13}C NMR (100 MHz, CDCl$_3$): δ = 150.2, 136.1, 132.5, 131.4, 118.1, 106.6, 104.7, 102.5, 56.7, 18.2, 12.9; HRMS (ESI): *m/z* [M+H]$^+$ calcd for C$_{18}$H$_{29}$BrNOSi$^+$: 382.1196 and 384.1176; found: 382.1198 and 384.1175.

6-Bromo-3-iodo-5-methoxy-1-(triisopropylsilyl)-1*H*-indole (13)

Protected bromoindole **11** (315 mg, 0.824 mmol) was dissolved in pyridine (0.5 mL) and the solution was cooled to 0 °C before ICl (1M in CH$_2$Cl$_2$, 0.90 mL, 0.90 mmol) was added slowly by syringe. After 15 min stirring at 0 °C, the cooling bath was removed and stirring continued for 30

min at rt. The reaction mixture was quenched with cold water (2 mL), diluted with ethyl acetate (20 mL) and HCl (1M, 3 mL) was added. The layers were separated and the aqueous layer was extracted with EtOAc (2 x 20 mL), and the combined organic phase was washed with saturated NaCl (20 mL) before it was dried over $MgSO_4$ and concentrated under vacuum. The residue was purified by flash chromatography (hexane to hexane/EtOAc, 98:2 v/v) to give the title compound **13** (451 mg, 97%) as a colorless solid. R_f (hexane/EtOAc, 98:2 v/v) = 0.30; ^1H NMR (500 MHz, $CDCl_3$): δ = 7.66 (s, 1H), 7.25 (s, 1H), 6.91 (s, 1H), 3.98 (s, 3H), 1.64 (hept, J = 7.5 Hz, 3H), 1.14 (d, J = 7.5 Hz, 18H); ^{13}C NMR (126 MHz, $CDCl_3$): δ = 151.1, 136.1, 135.3, 133.0, 118.3, 108.1, 102.7, 59.7, 56.7, 18.1, 12.8; HRMS (ESI): m/z [M+H]$^+$ calcd for $C_{18}H_{28}BrINOSi^+$: 508.0163 and 510.0142; found: 508.0161 and 510.0139.

5-(6-Bromo-5-methoxy-1-(triisopropylsilyl)-1*H*-indol-3-yl)oxazole (14)

3-Iodoindole **13** (0.55 g, 1.08 mmol), K_3PO_4 (0.689 g, 3.25 mmol) and 2-TIPS-oxazole-5-boronic acid pinacol ester (456 mg, 1.30 mmol) were dissolved in water (4.0 mL) and toluene (8.0 mL) and the mixture was degassed. $PdCl_2(dppf)\cdot CH_2Cl_2$ (44 mg, 0.054 mmol) was added and the mixture was degassed with argon before it was heated at 50 °C for 2 h. The reaction mixture was cooled to rt, diluted with EtOAc (20 mL), filtered through a short plug of celite, added the water (20 mL) and extracted with EtOAc (3 x 20 mL). The combined organic layers were washed with water (20 mL), saturated NaCl (20 mL), dried over $MgSO_4$ and concentrated under reduced pressure. The residue was dissolved in THF (10.0 mL) and aliquots of aqueous HCl (3 M, 2.0 mL) were added every 15 minutes for 1 h until the intermediate product could not be observed by TLC analysis (hexane/EtOAc, 4:1 v/v). The mixture was basified by addition of saturated $NaHCO_3$ (4.0 mL), partitioned between water and EtOAc (20 mL). The organic layer was washed with water (15 mL)

and saturated NaCl (15 mL), dried over MgSO$_4$ and evaporated under reduced pressure. The crude product was purified by flash chromatography (hexanes to hexanes/EtOAc, 3:1 v/v) to give the title compound **14** (303 mg, 62% over two steps) as a colorless thick oil. R$_f$ (hexanes/EtOAc, 3:1 v/v) = 0.35; ^{1}H NMR (500 MHz, CDCl$_3$): δ = 7.91 (s, 1H), 7.70 (s, 1H), 7.52 (s, 1H), 7.28 (s, 1H), 7.24 (s, 1H), 3.98 (s, 3H), 1.70 (sept, J = 7.5 Hz, 3H), 1.16 (d, J = 7.5 Hz, 18H); ^{13}C NMR (126 MHz, CDCl$_3$): δ = 151.2, 149.1, 147.7, 136.4, 130.2, 127.5, 119.7, 118.7, 107.9, 107.4, 101.7, 56.8, 18.1, 12.8; HRMS (ESI): m/z [M+H]$^+$ calcd for C$_{21}$H$_{30}$BrN$_2$O$_2$Si$^+$: 449.1254 and 451.1234; found: 449.1254 and 449.1232.

5-(6-Bromo-1-(triisopropylsilyl)-1H-indol-3-yl)-2,4-iodooxazole (15)

A solution of oxazole **14** (270 mg, 0.600 mmol) in THF (4.0 mL) was cooled to -78 °C, and LiHMDS (1M, 2.0 mL, 2.0 mmol) was added drop-wise and stirring continued at -78 °C for 1 h. A solution of iodine (305 mg, 1.20 mmol) in THF (2.0 mL) was added dropwise and stirring was continued at -78 °C for 30 min and then the reaction mixture was allowed to warm up to -40 °C and stirred for 1 h. A 10% aqueous solution of Na$_2$S$_2$O$_3$ (2.0 mL) was added and the resulting mixture was diluted with water (20 mL) and the resulting mixture was extracted with EtOAc (3 x 15 mL). The combined organic layers were washed with saturated NaCl (15 mL), dried over MgSO$_4$ and concentrated under reduced pressure. The resulting crude product was purified using flash chromatography to give the title compound **15** (129 mg, 31%) as colorless solid along with a mixture of 2-iodooxazole **16** and 4-iodooxazole **17** (162 mg, 47%). R$_f$ (hexanes/EtOAc, 3:1 v/v) = 0.37; ^{1}H NMR (500 MHz, CDCl$_3$): δ = 7.98 (s, 1H), 7.70 (s, 1H), 7.44 (s, 1H), 3.98 (s, 3H), 1.68 (p, J = 7.5 Hz, 3H), 1.17 (d, J = 7.5 Hz, 18H); ^{13}C NMR (126 MHz, CDCl$_3$): δ = 156.0, 151.3,

135.9, 132.2, 128.0, 118.5, 108.2, 105.3, 102.6, 97.9, 77.2, 56.7, 18.1, 12.8.; HRMS (ESI): m/z [M+H]$^+$ calcd for $C_{21}H_{28}BrI_2N_2O_2Si^+$: 700.9187 and 702.9193; found: 701.0977 and 703.0955.

tert-Butyl 2-(5-(6-bromo-1-(triisopropylsilyl)-1_H_-indol-3-yl)-4-iodooxazol-2-yl)-1_H_-pyrrole-1-carboxylate (18)

To a suspension of diiodo oxazole **15** (115 mg, 0.164 mmol), _N_-Boc-pyrrole-2-boronic acid (52 mg, 0.246 mmol) and Cs_2CO_3 (160 mg, 0.492 mmol) in 1,4-dioxane (4 mL) and water (1 mL), Pd(dppf)Cl$_2$•CH$_2$Cl$_2$ (13 mg, 0.016 mmol) was added and the resulting solution degassed with argon for 10 min and then stirred at rt for 48 h. The reaction mixture was concentrated in vacuo at 20 °C, diluted with EtOAc (15 mL) and water (10 mL). The organic layer was separated, washed with saturated NaCl, dried over $MgSO_4$ and concentrated under vacuum. The crude product was purified by flash chromatography (hexanes/EtOAc, 5:1 v/v to 3:1 v/v) to give the title compound **18** (80 mg, 66%) as colorless solid. R$_f$ (hexanes/EtOAc, 3:1 v/v) = 0.25; ^{1}H NMR (500 MHz, CDCl$_3$): δ = 8.08 (s, 1H), 7.69 (s, 1H), 7.53 (s, 1H), 7.46 (dd, J = 3.3, 1.8 Hz, 1H), 6.78 (dd, J = 3.5, 1.8 Hz, 1H), 6.31 (t, J = 3.4 Hz, 1H), 3.92 (s, 3H), 1.69 (p, J = 7.5 Hz, 3H), 1.41 (s, 9H), 1.18 (d, J = 7.5 Hz, 18H); ^{13}C NMR (126 MHz, CDCl$_3$): δ = 155.2, 151.2, 149.4, 148.5, 136.0, 132.4, 128.1, 125.0, 120.4, 119.1, 118.4, 111.2, 108.2, 106.2, 103.3, 85.0, 76.5, 57.0, 27.9, 18.2, 12.9.

Materials and methods for bioactivity assays

MTS assay

The cytotoxicities of compounds **1** – **6** were determined against the human cancer cell lines MCF-7 (breast adenocarcinoma, American Type Culture Collection (ATCC) HTB-22), HT29 (colon adenocarcinoma, ATCC HTB-38), A2058 (melanoma, ATCC = CRL-11147), MDA-MB-468

(breast adenocarcinoma, ATCC = HTB-132), SK-BR-3 (breast adenocarcinoma, ATCC = HTB-30), MOLT-4 (acute lymphoblastic leukemia, ATCC = CRL-1582) and MV-4-11 (biphenotypic B myelomonocytic leukemia, ATCC = CRL-9591), and MRC5 (non-malignant human lung fibroblasts, ATCC CCL-171) using the MTS assay.[23] HT-29 and MOLT-4 were cultured in RPMI, MCF-7 and MRC-5 in E-MEM, A2058 in D-MEM, MDA-MB-468 in L15, SK-BR-3 in McCoy's 5A and MV-4-11 in Iscove basal medium. All cell lines were assayed in RPMI. All cells were incubated in 5% CO2 at 37 ˚C. When assayed, the adherent cell lines were seeded in 96-well microtiter plates at 2000 cells/well for MCF-7, HT-29 and A2058, 5000 cells/well for MDA-MB-468 and SK-BR-3 and 4000 cells/well for MRC-5. After 24 h, each cancer cell line were treated with various concentrations of compounds **1 - 6** and incubated for 72 h. The suspension cell liens MOLT-4 and MV-4-11 were seeded at 10.000 cells/well and were immediately treated with various concentrations of compounds **1 – 6** and incubated for 72 h. The negative control was RPMI with 1% DMSO (1% was the highest DMSO concentration used in compound wells). Positive control for MCF-7, HT-29, A2058 and MRC-5 was 0.5% Triton X-100 (Sigma-Aldrich). Positive control for MDA-MB-468, SK-BR-3, MOLT-4 and MV-4-11 was RPMI with 10% DMSO. After 72 h, 10 µL of MTS solution (Cell Titter 96 Aqueous One Solution Reagent, Promega) was added to each well, and the cells were incubated for 1 h at 37 ˚C. The absorbance was measured at 485 nm using a DTX multimode detector (Beckman Coulter). Cell viability was calculated as follows: Cell survival (%) = (Absorbance treated wells – absorbance positive control)/(absorbance negative control – absorbance positive control) * 100. The half-maximal inhibitory concertation (IC_{50}) was calculated using Graph Pad Prism software. The time dependency of the activity of 3 against HT-29 and 4 against MCF-7 was further evaluated. Cells were added ranging concentrations of **3** and **4** 80, 60 and 36 h after seeding to evaluate the effect of the compounds after 4, 24 and 48 h exposure

times. Results were measured and evaluated as described above. All viability assays were performed in triplicate in three independent experiments.

^{33}P-ATP filter binding kinase assay

1, **3** and **4** were tested against 140 kinases in the Premier Screen kinase panel at the International Centre for Kinase Profiling using radioactive (^{33}P-ATP) filter-binding assays.[24] Compound **1** was tested at a concentration of 50 µM, **3** at 50, 5 and 1 µM, **4** at 5 and 1 µM. Each experiment was conducted in duplicates. Furthermore, the IC$_{50}$ values against 13 relevant kinases were determined for **2** – **6**. The experiments are run as a single 10-point concentration curve.

Active-site directed competition binding assay

The binding interactions between **3** at 10 µM and 468 kinases were determined using the ScanMax kinase panel at DiscoverX.[30, 31] In these assays, the ability of a compound to bind to the active site of the kinase is measures. Binding prevents the kinase from binds to an immobilized ligand, thereby reducing the amount of kinase captured by a solid bead. The kinases are labelled with a DNA tag. The amount of kinase captured by the solid bead us quantified by qPCR detecting the DNA tags. The binding affinities are reported as Percent of Control (% Ctrl) and are calculated by comparing captured kinase levels in test compound wells, negative control wells (DMSO) and positive control (control compounds) using the following equation: ((test compound signal – positive control signal)/(negative control signal – positive control signal) * 100 = % Ctrl. The binding constant (K$_d$) of **3** against 19 selected kinases were determined using K$_d$ELECT screening service at DiscoverX using 11-point dose response curves. Assay principle as described above. K$_d$ values were calculated using the Hill equation.

In vitro ATP competitiveness assay

The compounds were diluted in 50 mM HEPES (pH 7.5), 10 mM MgCl$_2$, 1 mM EGTA and 0.01% Brij35. The kinase of interest (5 nM final concentration), fluorescent tracer (Invitrogen, 100 nM final concentration) and LanthaScreen Eu-anti-GST antibody (Invitrogen, 2 nM final concentration) were mixed with the respective compound dilutions (from 5 nM to 10 mM) and incubated for 1 h. The FRET signal was quantified using an EnVision Multilabellreader 2104 (Perkin Elmer).[46]

Intracellular ATP competitiveness assays

In brief, HEK293 cells were seeded in 384 well plates and transfected with plasmids for expression of DRAK1 or DRAK2 fused to the NanoLuc luciferase. 24 h post transfection, cells were washed, permeabilized with digitonin, and treated with an ATP-competitive tracer according to the Manufacturer's instructions.[47]

Docking

In brief, the binding mode of **3** into the ATP-binding pocket of PIM1 was determined by manual and computational docking using the Glide software from Schrödinger. Protein coordinates were extracted from the crystal structure of the structure of PIM1 bound to N-(5-(2-fluorophenyl)-1H-pyrrolo[2,3-b]pyridin-3-yl)-5-((((3R,4R)-3-fluoropiperidin-4-yl)methyl)amino)pyrazolo[1,5-a]pyrimidine-3-carboxamide (PDB code: 4K1B).

Selective cytotoxicity

Compound **3** was assayed against the cell lines found in the OncoLead cell panel using a sulforhodamin B (SRB) protein staining assay technique[37] (Oncolead, Karlsfeld, Germany). Cancer

cells (87 in total) and peripheral blood mononuclear cells (PBMCs) were assayed. Briefly, 24 h post seeding, cells were treated in triplicate with a 10-fold serial dilution over 10 concentrations of **3**. The highest assayed concentration was 30 µM. Following 72 h incubation, cells growth inhibitions were measured using SRB in a protein staining assay. Results were used to calculate the IC_{50} value of **3** against the 88 cell lines.

Polypharmacological effects

The polypharmacological effects of **3** were evaluated using the CEREP Panlab Diversity Panel. The purpose of this panel of binding and cellular assays performed by CEREP is to identify a subset of potential receptors, transporters, ion channels, etc, for which a compound displays affinity. The panel includes radioligand binding- and cell based assays, which are run as described by the service provider. The results are expressed as percent-of-control specific binding.

In vivo toxicity against zebrafish embryos

BioReperia (Linköping, Sweden) conducted assays to evaluate the toxicological properties of compound **3** against zebrafish embryos. Zebrafish embryos were produced by natural breeding from two males and four females, collected, screened for fertilization and moved to E4 medium. Embryos were incubated and at 28.5 °C. After fertilization (4 h) the embryos were allocated into six groups of 20 individuals. Unfertilized eggs or embryos that did not appear healthy or exhibited any obvious developmental defects were excluded prior to treatment onset at 4 hours after fertilization of the egg. The assays were conducted at five concentrations (1396, 140, 14, 1.4 and 0.1 µM). Vehicle (DMSO) was given at 0.5%, corresponding to the highest concentration in the treatment group.

Determination of ADME parameters

Chemical stability assay

Chemical stability was determined by incubating test compounds at a final concentration of 2 µM in aqueous buffer at pH 7.4 for 1, 7 and 24 h, respectively. The percentage of remaining compound in relation to the zero time point was calculated following LCMS-based measurement of sample aliquots of each time point.

Stability in cell culture medium assay

Stability in cell culture medium was determined by incubating compound **3** at a final concentration of 2 µM in D-MEM supplemented with 10% fetal calf serum at pH 7.4 for 1, 7 and 24 h, respectively. The percentage of remaining compound in relation to the zero time point was calculated following LCMS-based measurement of sample aliquots of each time point.

Kinetic solubility assay

Aqueous solubility of compounds was determined by spectrophotometrical measurement of the kinetic solubility of a 500 µM compound solution in aqueous buffer pH 7.4 compared to a solution in the organic solvent acetonitrile after 90 min of vigorous shaking at room temperature.

Permeability through artificial membranes assay

Permeability through artificial membranes (PAMPA) was performed at an initial concentration of 500 µM of the compound in the donor compartment. After an incubation period of 20 h, absorption of the receiver wells was measured by spectrophotometry and permeation was calculated by normalization of the compound flux across a blank filter.

Microsomal stability phase I assay

Metabolic stability under oxidative conditions was measured in liver microsomes from different species by LCMS-based measuring of depletion of compound at a concentration of 3 µM over time up to 50 min at 37 °C. Based on compound half-life $t_{1/2}$, in vitro intrinsic clearance CL_{int} was calculated. $Cl_{int} = (V \times 0.693)/(t_{1/2} \times mg)$

Microsomal stability phase II assay

Metabolic stability under conjugative conditions was measured in the glucuronidation assay by LCMS-based determination of % remaining of selected compounds at a concentration of 5 µM in incubations with liver microsomes supplemented with UDP-glucuronic acid for 1h at 37 °C.

Plasma Stability assay

Plasma stability was measured by LCMS-based determination of % remaining of selected compounds at a concentration of 5 µM after incubation in 100% plasma obtained from different species for 1 h at 37 °C.

Plasma Protein Binding assay

Assessment of plasma protein binding was measured by equilibrium dialysis by incubating the compound of interest at a concentration of 5 µM for 6 h at 37 °C in 50% plasma in buffer (v/v) followed by LCMS-based determination of final compound concentrations. The resulting fraction unbound at 50% plasma ($fu_{50\%}$) is extrapolated to the fraction unbound at 100% plasma ($fu_{100\%}$) using the following equation: $fu_{100\%} = fu_{50\%}/(2 - fu_{50\%})$

AUTHOR INFORMATION

Corresponding Authors

*E-mail: Kine.O.Hanssen@uit.no
*E-mail: Bengt-Erik.Haug@uib.no

Author Contributions

K.Ø.H. and E.H.H. isolated the compounds. J.I. and E.H.H. performed the analytical characterization of the isolated compounds. K.Ø.H. performed the *In Vitro* Cytotoxicity assays. S.K.P., M.L., B.E.H., A.B., K.B.J., M.O.S. and Y.G. planned and conducted the synthesis and characterized the synthetic products. B.K. and J.E. performed the mode-of-action studies. M.B. measured the *In Vitro* ADME parameters. U.K. performed the docking study. The manuscript was written through contributions of all authors. All authors have given approval to the final version of the manuscript.

Notes

The authors declare no competing financial interest.

ACKNOWLEDGMENT

ABBREVIATIONS

GC, Gini coefficient; RA, residual enzyme activities; PoC, percent of control, ICKP, International Centre for Kinase Profiling in Dundee, TIPS, triisopropyl ether; TBS, *t*-butyldimethylsilyl.

Supporting Information

The Supporting Information is available free of charge on the ACS Publication website at DOI:

Molecular formula strings (CSV)

Supporting information file 1: NMR spectra for compounds **3** – **8**, synthetic intermediates towards **3**, synthetic **3** and **4**, isolated **1** and **2**, and comparison of ^{1}H- and ^{13}C-NMR data for isolated and synthetic **3** and **4**.

Supporting information file 2: The activities of **1**, **3** and **4** against 140 kinases using a radioactive (^{33}P-ATP) filter-binding assays, binding affinity of **3** against the 468 kinases in the DiscoverX ScanMax panel, diversity profile of **3**, IC$_{50}$ values of **3** against the 88 cell lines found in the OncoLead panel, TreeSpot analysis of **3** at 5 µM based on Discoverx data, curve images for K$_{d}$ determination of **3**, dose-response-time curves for **3** against HT-29 and **4** against MCF-7.

REFERENCES

1.   Bhullar, K. S.; Lagarón, N. O.; McGowan, E. M.; Parmar, I.; Jha, A.; Hubbard, B. P.; Rupasinghe, H. P. V. Kinase-targeted cancer therapies: progress, challenges and future directions. Mol. Cancer 2018, 17, 48.

2.   Kolch, W.; Halasz, M.; Granovskaya, M.; Kholodenko, B. N. The dynamic control of signal transduction networks in cancer cells. Nat. Rev. Cancer 2015, 15, 515-527.

3.   Brognard, J.; Hunter, T. Protein kinase signaling networks in cancer. Curr. Opin. Genet. Dev. 2011, 21, 4-11.

4.   Gross, S.; Rahal, R.; Stransky, N.; Lengauer, C.; Hoeflich, K. P. Targeting cancer with kinase inhibitors. J. Clin. Invest. 2015, 125, 1780-1789.

5.   Sawyers, C. Targeted cancer therapy. Nature 2004, 432, 294-297.

6.   Kroschinsky, F.; Stolzel, F.; von Bonin, S.; Beutel, G.; Kochanek, M.; Kiehl, M.; Schellongowski, P. New drugs, new toxicities: severe side effects of modern targeted and immunotherapy of cancer and their management. Crit. Care. 2017, 21, 89.

7.   Roskoski, R., Jr. Classification of small molecule protein kinase inhibitors based upon the structures of their drug-enzyme complexes. Pharmacol. Res. 2016, 103, 26-48.

8.   Wu, P.; Nielsen, T. E.; Clausen, M. H. Small-molecule kinase inhibitors: an analysis of FDA-approved drugs. Drug. Discov. Today 2016, 21, 5-10.

9.   Hanssen, K. O.; Schuler, B.; Williams, A. J.; Demissie, T. B.; Hansen, E.; Andersen, J. H.; Svenson, J.; Blinov, K.; Repisky, M.; Mohn, F.; Meyer, G.; Svendsen, J. S.; Ruud, K.; Elyashberg, M.; Gross, L.; Jaspars, M.; Isaksson, J. A combined atomic force microscopy and computational approach for the structural elucidation of breitfussin A and B: Highly modified halogenated dipeptides from Thuiaria breitfussi. Angew. Chem. Int. Edit. 2012, 51, 12238-12241.

10.   Pandey, S. K.; Guttormsen, Y.; Haug, B. E.; Hedberg, C.; Bayer, A. A concise total synthesis of breitfussin A and B. Org. Lett. 2015, 17, 122-125.

11.   Rudi, A.; Stein, Z.; Green, S.; Goldberg, I.; Kashman, Y.; Benayahu, Y.; Schleyer, M. Phorbazoles A-D, novel chlorinated phenylpyrrolyloxazoles from the marine sponge phorbas aff. clathrata. Tetrahedron Lett. 1994, 35, 2589-2592.

12.   Lindquist, N.; Fenical, W.; Van Duyne, G. D.; Clardy, J. Isolation and structure determination of diazonamides A and B, unusual cytotoxic metabolites from the marine ascidian Diazona chinensis. J. Am. Chem. Soc. 1991, 113, 2303-2304.

13.   Takahashi, S.; Matsunaga, T.; Hasegawa, C.; Saito, H.; Fujita, D.; Kiuchi, F.; Tsuda, Y. Martefragin A, a novel indole alkaloid isolated from red alga, inhibits lipid peroxidation. Chem. Pharm. Bull. 1998, 46, 1527-1529.

14.   Pettit, G. R.; Knight, J. C.; Herald, D. L.; Davenport, R.; Pettit, R. K.; Tucker, B. E.; Schmidt, J. M. Isolation of Labradorins 1 and 2 from Pseudomonas syringae pv. coronafaciens. J. Nat. Prod. 2002, 65, 1793-1797.

15.   Liu, K. Total synthesis of CPI-2081, breitfussin B and synthetic studies towards myriastramide C and goadsporin. University of East Anglia, 2015.

16.   Khan, A. H.; Chen, J. S. Synthesis of breitfussin B by late-stage bromination. Org. Lett. 2015, 17, 3718-3721.

17.   Cambeiro, X. C.; Ahlsten, N.; Larrosa, I. Au-catalyzed cross-coupling of arenes via double C–H activation. J. Am. Chem. Soc. 2015, 137, 15636-15639.

18.   Pelkey, E. T. Metalation of Indole. In Heterocyclic Scaffolds II: Reactions and Applications of Indoles, Gribble, G. W., Ed. Springer: Berlin, Heidelberg, 2010; pp 141-191.

19.   Sundberg, R. J.; Parton, R. L. Lithiation of methoxyindoles. J. Org. Chem. 1976, 41, 163-165.

20.   Snieckus, V. Directed ortho metalation. Tertiary amide and O-carbamate directors in synthetic strategies for polysubstituted aromatics. Chem. Rev. 1990, 90, 879-933.

21.   Nirogi, R.; Adireddy, D.; Bhatta, V.; Kota, L.; Dubey, P. K. Synthesis and structure activity relationship of rigidized indolyl pyrrolidine derivatives as 5-HT6 receptor ligands. Asian J. Chem. 2013, 25, 9293-9298.

22.   Griffen, E. J.; Roe, D. G.; Snieckus, V. Benzenoid ring functionalization of indoles and tryptophols via combined directed ortho metalation-cross coupling methodology. J. Org. Chem. 1995, 60, 1484-1485.

23.   Riss, T. L.; Moravec, R. A.; Niles, A. L.; Duellman, S.; Benink, H. A.; Worzella, T. J.; Minor, L. Cell viability assays. In Assay Guidance Manual, Eli Lilly & Company and the National Center for Advancing Translational Sciences: 2016.

24.   Hastie, C. J.; McLauchlan, H. J.; Cohen, P. Assay of protein kinases using radiolabeled ATP: a protocol. Nat. Protoc. 2006, 1, 968-971.

25.   Graczyk, P. P. Gini Coefficient: A new way to express selectivity of kinase inhibitors against a family of kinases. J. Med. Chem. 2007, 50, 5773-5779.

26.   Uitdehaag, J. C.; Zaman, G. J. A theoretical entropy score as a single value to express inhibitor selectivity. BMC bioinformatics 2011, 12, 94.

27.   Karaman, M. W.; Herrgard, S.; Treiber, D. K.; Gallant, P.; Atteridge, C. E.; Campbell, B. T.; Chan, K. W.; Ciceri, P.; Davis, M. I.; Edeen, P. T.; Faraoni, R.; Floyd, M.; Hunt, J. P.; Lockhart, D. J.; Milanov, Z. V.; Morrison, M. J.; Pallares, G.; Patel, H. K.; Pritchard, S.; Wodicka, L. M.; Zarrinkar, P. P. A quantitative analysis of kinase inhibitor selectivity. Nature biotechnology 2008, 26, 127.

28.   Saurabh, K.; Scherzer, M. T.; Shah, P. P.; Mims, A. S.; Lockwood, W. W.; Kraft, A. S.; Beverly, L. J. The PIM family of oncoproteins: small kinases with huge implications in myeloid leukemogenesis and as therapeutic targets. Oncotarget 2014, 5, 8503-8514.

29.   Willems, E.; Dedobbeleer, M.; Digregorio, M.; Lombard, A.; Lumapat, P. N.; Rogister, B. The functional diversity of Aurora kinases: a comprehensive review. Cell div. 2018, 13, 7.

30.   Fabian, M. A.; Biggs, W. H., 3rd; Treiber, D. K.; Atteridge, C. E.; Azimioara, M. D.; Benedetti, M. G.; Carter, T. A.; Ciceri, P.; Edeen, P. T.; Floyd, M.; Ford, J. M.; Galvin, M.; Gerlach, J. L.; Grotzfeld, R. M.; Herrgard, S.; Insko, D. E.; Insko, M. A.; Lai, A. G.; Lelias, J. M.; Mehta, S. A.; Milanov, Z. V.; Velasco, A. M.; Wodicka, L. M.; Patel, H. K.; Zarrinkar, P. P.; Lockhart, D. J. A small molecule-kinase interaction map for clinical kinase inhibitors. Nat. Biotechnol. 2005, 23, 329-336.

31.   Miduturu, C. V.; Deng, X.; Kwiatkowski, N.; Yang, W.; Brault, L.; Filippakopoulos, P.; Chung, E.; Yang, Q.; Schwaller, J.; Knapp, S.; King, R. W.; Lee, J.-D.; Herrgard, S.; Zarrinkar, P.; Gray, N. S. High-throughput kinase profiling: A more efficient approach towards the discovery of new kinase inhibitors. Chem. biol. 2011, 18, 868-879.

32.   Rudolf, A. F.; Skovgaard, T.; Knapp, S.; Jensen, L. J.; Berthelsen, J. A comparison of protein kinases inhibitor screening methods using both enzymatic activity and binding affinity determination. PloS one 2014, 9, e98800.

33.   Brasó-Maristany, F.; Filosto, S.; Catchpole, S.; Marlow, R.; Quist, J.; Francesch-Domenech, E.; Plumb, D. A.; Zakka, L.; Gazinska, P.; Liccardi, G.; Meier, P.; Gris-Oliver, A.; Cheang, M. C. U.; Perdrix-Rosell, A.; Shafat, M.; Noël, E.; Patel, N.; McEachern, K.; Scaltriti, M.; Castel, P.; Noor, F.; Buus, R.; Mathew, S.; Watkins, J.; Serra, V.; Marra, P.; Grigoriadis, A.; Tutt, A. N. PIM1 kinase regulates cell death, tumor growth and chemotherapy response revealing a novel target in triple-negative breast cancer. Nat. Med. 2016, 22, 1303-1313.

34.   Daver, N.; Schlenk, R. F.; Russell, N. H.; Levis, M. J. Targeting FLT3 mutations in AML: review of current knowledge and evidence. Leukemia 2019, 33, 299-312.

35.   Wu, D.-D.; Lau, A.; Yu, F.-Y.; Cai, N.-L.; Dai, L.-J.; Ok Kim, M.; Jin, D.-Y.; Xu, Y.-M. Extracellular signal-regulated kinase 8-mediated NF-kappaB activation increases sensitivity of human lung cancer cells to arsenic trioxide. Oncotarget 2017, 8, 49144-49155.

36.   Chieffi, P. Aurora B: A new promising therapeutic target in cancer. Intractable Rare Dis Res 2018, 7, 141-144.

37.   Vichai, V.; Kirtikara, K. Sulforhodamine B colorimetric assay for cytotoxicity screening. Nature protocols 2006, 1, 1112-1116.

38.   Raynaud, F. I.; Whittaker, S. R.; Fischer, P. M.; McClue, S.; Walton, M. I.; Barrie, S. E.; Garrett, M. D.; Rogers, P.; Clarke, S. J.; Kelland, L. R.; Valenti, M.; Brunton, L.; Eccles, S.; Lane, D. P.; Workman, P. In vitro and In vivo pharmacokinetic-pharmacodynamic relationships for the trisubstituted aminopurine cyclin-dependent kinase inhibitors olomoucine, bohemine and CYC202. Clin. Cancer Res. 2005, 11, 4875-4887.

39.   Aslantürk, Ö. S. In vitro cytotoxicity and cell viability assays: principles, advantages, and disadvantages. InTech: 2018; Vol. 2.

40.   Wang, P.; Henning, S. M.; Heber, D. Limitations of MTT and MTS-based assays for measurement of antiproliferative activity of green tea polyphenols. PloS one 2010, 5, e10202-e10202.

41.   Sieuwerts, A. M.; Klijn, J. G.; Peters, H. A.; Foekens, J. A. The MTT tetrazolium salt assay scrutinized: how to use this assay reliably to measure metabolie activity of cell cultures in vitro for the assessment of growth characteristics, IC50-values and cell survival. Clin. Chem. Lab. Med. 1995, 33, 813-824.

42.   Xiao, Z.; Morris-Natschke, S. L.; Lee, K.-H. Strategies for the optimization of natural leads to anticancer drugs or drug candidates. Med. Res. Rev. 2016, 36, 32-91.

43.   Bharate, S. B.; Kumar, V.; Jain, S. K.; Mintoo, M. J.; Guru, S. K.; Nuthakki, V. K.; Sharma, M.; Bharate, S. S.; Gandhi, S. G.; Mondhe, D. M.; Bhushan, S.; Vishwakarma, R. A. Discovery and preclinical development of IIIM-290, an orally active potent cyclin-dependent kinase Inhibitor. J. Med. Chem. 2018, 61, 1664-1687.

44.   Jain, S. K.; Bharate, S. B.; Vishwakarma, R. A. Cyclin-dependent kinase inhibition by flavoalkaloids. Mini. Rev. Med. Chem. 2012, 12, 632-649.

45.   Sanjo, H.; Kawai, T.; Akira, S. DRAKs, novel serine/threonine kinases related to death-associated protein kinase that trigger apoptosis. J. Biol. Chem. 1998, 273, 29066-29071.

46.   Lebakken, C. S.; Riddle, S. M.; Singh, U.; Frazee, W. J.; Eliason, H. C.; Gao, Y.; Reichling, L. J.; Marks, B. D.; Vogel, K. W. Development and applications of a broad-coverage, TR-FRET-based kinase binding assay platform. J. Biomol. Screen. 2009, 14, 924-935.

47.   Vasta, J. D.; Corona, C. R.; Wilkinson, J.; Zimprich, C. A.; Hartnett, J. R.; Ingold, M. R.; Zimmerman, K.; Machleidt, T.; Kirkland, T. A.; Huwiler, K. G.; Ohana, R. F.; Slater, M.; Otto, P.; Cong, M.; Wells, C. I.; Berger, B. T.; Hanke, T.; Glas, C.; Ding, K.; Drewry, D. H.; Huber, K. V. M.; Willson, T. M.; Knapp, S.; Muller, S.; Meisenheimer, P. L.; Fan, F.; Wood, K. V.; Robers, M. B. Quantitative, wide-spectrum kinase profiling in live cells for assessing the effect of cellular ATP on target engagement. Cell. Chem. Biol. 2018, 25, 206-214.

48.   Sipes, N. S.; Padilla, S.; Knudsen, T. B. Zebrafish: as an integrative model for twenty-first century toxicity testing. Birth Defects Res. C. 2011, 93, 256-267.

FOR TABLE OF CONTENTS ONLY

NEW KINASE INHIBITION SCAFFOLD FROM THE ARCTIC, MARINE ENVIRONMENT

Natural products

T. breitfussi

Top candidate (3)

PIM1: IC_{50} = 200 nM

Mode-of-action studies

MDA-MB-468: IC_{50} = 340 nM